Hydrometeorological droughts in the Miño-Limia-Sil hydrographic demarcation (NW Iberian Peninsula): The role of atmospheric drivers

Rogert Sorí[1,2], Marta Vázquez[1,2,3], Milica Stojanovic[2,3], Raquel Nieto[1], Margarida Liberato[2,3], Luis Gimeno[1],

[1]Environmental Physics Laboratory (EPhysLab), CIM-UVigo, Universidade de Vigo, Ourense, 32004 Spain

[2]Instituto Dom Luiz, Faculdade de Ciências da Universidade de Lisboa, Campo Grande, Portugal

[3]Escola de Ciências e Tecnologia, Universidade de Trás-os-Montes e Alto Douro, Vila Real, Portugal

Correspondence to: Rogert Sorí (rogert.sori@uvigo.es)

Abstract. Drought is one of the main natural hazards because of its environmental, economic, and social impacts. Therefore, monitoring and prediction for small regions, countries, or whole continents are challenging. In this work, the meteorological droughts affecting the Miño-Limia-Sil Hydrographic Demarcation in the northwestern Iberian Peninsula during the period 1980–2017 were identified. For this purpose, and to assess the combined effects of temperature and precipitation on drought conditions, the Standardised Precipitation-Evapotranspiration Index was utilised. Some of the most severe episodes occurred during June 2016 – January 2017, September 2011 – March 2012, December 2014 – August 2015. An Empirical Orthogonal Function analysis for the Standardised Precipitation-Evapotranspiration Index series revealed that the spatial variability of the SPEI shows a great homogeneity in the region, and consequently the drought phenomenon behaves in the same way. Particular emphasis was given to investigating atmospheric circulation as a driver of different drought conditions. To this aim, a daily weather type classification based on Lamb weather type (LWT) classification (Lamb, 1972) was utilised for the entire Iberian Peninsula. The results showed that atmospheric circulation from the southwest, west, and northwest are directly related to wet conditions in the Miño-Limia-Sil Hydrographic Demarcation during the entire climatological year. Contrastingly, weather types imposing atmospheric circulation from the northeast, east, and southeast are best associated with dry conditions. Anomalies of the integrated vertical flow of humidity and their divergence for the onset, peak, and termination of the ten most severe drought episodes also confirmed these results. In this sense, the major atmospheric teleconnection patterns related to dry/wet conditions were the Arctic Oscillation, Scandinavian Pattern, and North Atlantic Oscillation. Hydrological drought investigated through the Standardised Runoff Index was closely related to dry/wet conditions revealed by the Standardised Precipitation-Evapotranspiration Index at shorter temporal scales, specially during the rainy season.

1. Introduction

Drought is one of the most dangerous natural phenomena in many regions worldwide, as it affects a wide range of environmental, economic, and social sectors (Wilhite, 2000; McMichael et al., 2011; Stankeet et al., 2013; Gerber and Mirzabaev, 2017; Liberato et al. 2017; Guerreiro et al., 2018). This phenomenon is usually considered a prolonged dry period in the natural water cycle that can occur anywhere in the world. It is initially caused by a lack of rainfall as well as for thermodynamics processes (e.g. radiative and turbulent fluxes and water phase transitions (Wehrli et al., 2018;) induced by the wind speed, temperature, relative humidity and solar and long-wave radiation (WMO & GWP, 2016; Vicente-Serrrano et al., 2010; Sereviratne, 2012; Miralles et al., 2019). Drought propagation is also due to natural and human drivers through multiples feedbacks (Van Loon et al., 2016). The Iberian Peninsula (IP) in the Euro-Atlantic and Mediterranean regions is a drought-prone area (Páscoa et al., 2017) that has been affected by well known record-breaking droughts in 2004-2005 (García-Herrera et al., 2007), 2011-2012 (Trigo et al., 2013), and 2015-2016 (García-Herrera et al., 2019). Temperature increase has been responsible for greater drought severity and larger surface area affected in the IP from 1980s to 2010 (respect 1906-2010) due to the increase in atmospheric evaporative demand (Coll et al., 2017). Concerning the existence of the trends in droughts a significant tendency towards dryness during 1901–1937 and 1975–2012 (Páscoa et al., 2017). Over a shorter study period (1974–2010), Gómez-Gesteira et al. (2011) found a significant increasing trend in land atmospheric and sea surface temperatures of 0.5 °C and 0.24 °C per decade, respectively, but annual P did not show any trend in the north western IP. The high confidence level that global warming is likely to reach 1.5 °C above preindustrial levels in a short period (between 2030 and 2052) if it continues to increase at the current rate is a nowadays concern (IPCC, 2018). In this sense, the IP is considered one of the European regions that is most likely to suffer an increase in drought severity during the 21st century (Spinioni et al., 2018). However, Trenberth et al. (2014) argued that increased heating from global warming may not cause droughts, but it is expected that when droughts occur they are likely to occur more quickly and be more intense.

Drought processes involve interactions amongst ocean processes (ocean teleconnections), land-based processes (water balance, runoff), and several atmospheric processes (Spinioni et al., 2017). Therefore, to investigate droughts and their impact on the availability of water resources in the IP have been used multiple methods and analysis such as the implementation of weather types classifications (WTs) (Cortesi et al., 2014; Ramos et al., 2014), identification of blocking events (Sousa et al., 2016), and assessments of climatic teleconnection patterns like the North Atlantic Oscillation (NAO) (Muñoz-Díaz and Rodrigo, 2004; Trigo et al., 2004; deCastro et al., 2006), which is considered a dominant mode of climate variability for Europe (Visbeck et al., 2001), the Arctic Oscillation (AO) (deCastro et al., 2006), El Niño Southern Oscillation (ENSO) (Vicente-Serrano, 2005), and the Scandinavian Pattern (SCAND) (deCastro et al., 2006). The impacts of drought have been widely investigated in the IP, and range from affecting the productivity of rainfed crops (Peña-Gallardo et al., 2019), forests (Gouveia et al., 2009; Barbeta and Peñuelas, 2016; Vidal-Macua et al., 2017; Peña-Gallardo et al., 2018), and even the human mortality in Galicia, northwestern Spain (Salvador et al., 2019). Terrestrial ecosystems often vary significantly in their responses to drought (Knapp

et al., 2015). Moreover, IP is characterised by different climate types, from a humid Atlantic climate in the northwest and north to semi-arid Mediterranean conditions in the east and southeast (Parracho et al., 2016), and strong seasonal variability (Serrano et al., 1999). Therefore, regional-scale studies have the advantage of better characterising the phenomenon of drought and its impacts, thereby supporting the reduction of the vulnerability and losses induced by drought.

The north western IP is a hydrologically important region where water resources of the Miño-Sil and Limia river basins represent an important source of benefits for inhabitants of Galicia and the northern provinces of Portugal. Both basins make up the Miño-Limia-Sil Hydrographic Demarcation (MLSHD) (Figure 1), a region of environmental shared resources for Spain and Portugal. The water resources in the MLSHD are crucial to develop agriculture and livestock. Indeed, in the Spanish part of the MLSHD, the water demands of agrarian use represent 73.2% of the total water demand (Vargas and Paneque, 2019). The industrial use of water for energy production is mainly carried out through hydroelectric and thermal power plants, which has caused hydromorphological alterations in the main rivers due to the construction of dams and dikes (CMS-PH, 2017). Indeed, the total installed power in the Spanish part is 4763 MW. Besides, the MLSHD also has recreational uses and a high ecosystem value. To the best of our knowledge, there are not any published drought studies considering the MLSHD as a whole. Therefore, in this study our main aim is to investigate the meteorological droughts that have affected the MLSHD, and evaluate the role of atmospheric circulation and large-scale teleconnection patterns in the occurrence and magnitude of droughts. We focus on meteorological droughts attempting to explain the primary causes of other types of droughts. The accuracy of drought forecasting is a challenge for hydroclimate sciences. Therefore, investigating drought characteristics and generating mechanisms is essential to take actions such as monitoring and early warnings, which contribute to efficient water management and reduction of the ecosystems and social vulnerability. We expect that our results will contribute to increase the hydroclimate knowledge of the MLSHD, support early warning, and strength drought management plans.

1.1 Study area

The MLSHD extends from approximately 42°N to 44°N and from 6.5°W to 9°W, and covers an area of approximately 20 000 km^2 in the NWIP (Figure 1), including the territories of Galicia (Spain) and northern Portugal. There are 191 municipalities of which 181 belong to the Spanish territory, and 10 in the Portuguese territory, with a total population of 1 084 636 people (by 2015) (Mora-Aliseda et al., 2015). It is considered a management unit where the terrestrial area is composed of the Miño-Sil and Limia river basins and the transitional, subterranean, and coastal waters associated with said basins (PES, 2017). The MLSHD is characterised by the presence of a diverse landscape; a diversity that is based on a complex relief structure and the Atlantic bioclimatic characters. The Miño-Sil basins have a pronounced mountainous character with an average elevation of about 683 m above sea level (UN, 2011), and the Lima River basin is 447 meters (CA, 2020). The coastline, valleys and mountains give it a wide variety of landscapes that are well differentiated both internally and with respect to other peninsular territories. In terms of the annual mean flow, the Miño-Sil river basin is the fourth largest basin in the Iberian Peninsula and because of that is important for hydropower generation (Lorenzo-Lacruz et al., 2012, Añel et al., 2013).

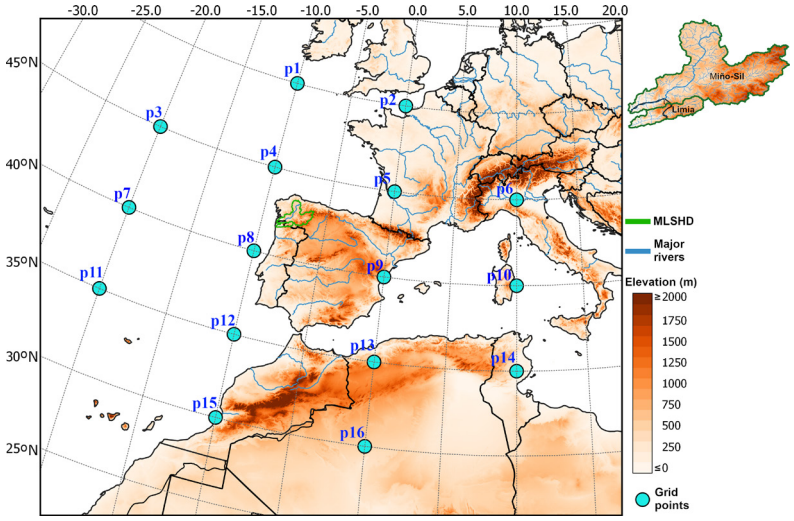

Figure 1. Geographic location and boundaries (green line) of the Miño-Sil and Limia River Basins which conform to the Miño-Limia-Sil Hydrographic Demarcation (MLSHD). The rivers are represented by blue lines and shaded reddish colours represent the elevation (in meters above sea level) from the HydroSHEDS project (Lehner et al., 2011). Light blue circles denote the location of the 16 points used to retrieve daily MSLP values for the circulation weather types (WTs) computation.

Its climate is characterized by mild winters, cool summers, humid air, abundant cloudiness and frequent rainfall in all seasons. The annual cycle of precipitation (P), maximum temperature (Tx), and minimum temperature (Tn) along the hydrological year (October of year n to September of year n+1) in the MLSHD using the E-OBS gridded dataset (Cornes et al., 2018) is shown in Figure 2. P presents a high temporal variability across the year, and is greater than 100 mm from October to February. During winter, the large-scale circulation is mainly driven by the position and intensity of the Iceland Low, and western Iberia is affected by westerly winds that bring humid air and generate P (Trigo et al., 2004). The movement of the sub-tropical anticyclone to the south leaves the region open to the influence of the frontal systems from the west, which are responsible for most of the P. Synoptic-scale baroclinic perturbations from the Atlantic Ocean are responsible for most of the P between October and May (DeCastro et al., 2006). After February, P is lower and reaches the minimum value (P < 30 mm) in July. Summer is predominantly influenced by high pressures, which determine air subsidence and consequently atmospheric stability (PGRH, 2016). The annual cycle of Tx and Tn revealed a cycle opposite to that of P. Minimum monthly values of Tx (< 9 °C) and Tn (2 °C) occur from December to February, while the maximum values occur in July and August (> 24 °C). Both the Miño and the Sil are remarkably regular rivers, although they have a maximum flow in winter (January and February) and a minimum in summer (August and September).

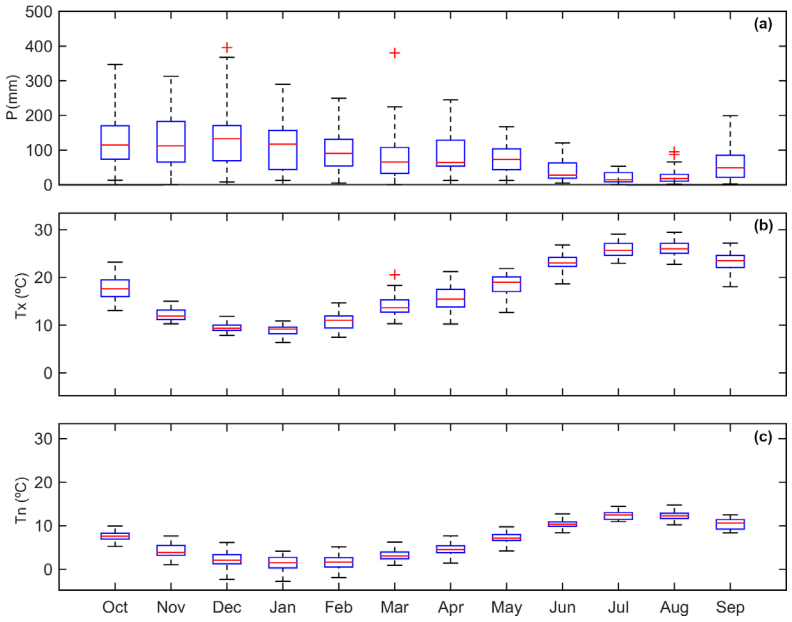

Figure 2. Annual cycle for the hydrological year spanning October of year n to September of year n+1, for the period 1980-2017, of monthly precipitation (a), maximum (b) and minimum (c) temperature in the Miño-Limia-Sil Hydrographic Demarcation, using the E-OBS gridded dataset. Boxes delineate median, upper and lower quartiles, with the whiskers representing the lowest and highest monthly value still within 1.5 of the interquartile range. +: outliers, i.e. values beyond the ends of the whiskers.

2. Material and methods

2.1 Datasets

Monthly gridded data of P, Tx and Tn were obtained from daily values of the E-OBS gridded dataset (Cornes et al., 2018) with a resolution of 0.1° in longitude and latitude for the period 1980–2017. This period was set for all the analyses in this study taking into account the simultaneous availability of data, and a period of more than 30 years. These series are also utilised to compute the SPEI in the MLSHD. For the WTs computation, daily values of SLP from the ERA-Interim reanalysis datasets (Dee et al., 2011) with a resolution of 1° considering 16 grid points shown in Figure 1 were utilised. The eastwards and northwards vertically integrated moisture flux from ERA-Interim was utilised to compute the Vertical Integral Moisture Flux (VIMF) anomalies and its divergence anomalies. Monthly values of runoff with a resolution of ~4-km monthly were freely downloaded from portal TerraClimate (Abatzoglou et al., 2018), available at http://www.climatologylab.org/terraclimate.html. TerraClimate uses climatically aided interpolation, combining high-spatial resolution climatological normals from the WorldClim dataset, with coarser spatial resolution, but time-varying data from CRU Ts4.0 and the Japanese 55-year Reanalysis (JRA55).

To identify the influence of short and large-scale modes of climate variability on the hydroclimate of the study region various datasets of teleconnection patterns are used. These are, the bivariate ENSO time series (BEST) (Smith and Sardeshmukh, 2000), (available at https://www.esrl.noaa.gov/psd/people/cathy.smith/best/) Western Mediterranean Oscillation (WeMO) (available at https://crudata.uea.ac.uk/cru/data/moi/), the North Atlantic Oscillation (NAO), Arctic Oscillation (AO), East Atlantic (EA), Scandinavia pattern (SCAND) (https://www.cpc.ncep.noaa.gov/data/teledoc/telecontents.shtml). The BEST index time series is based on the combination of the atmospheric component of the ENSO phenomenon (the Southern Oscillation Index or "SOI") and an oceanic component (average Nino 3.4 Sea Surface temperature). WeMO index (WeMOi) is based on the difference between the standardized atmospheric pressure recorded at Padua (45.40◦N, 11.48◦E) in northern Italy, and San Fernando, Cádiz (36.28◦N, 6.12◦W) in Southwestern Spain. To obtain the rest of Northern Hemisphere teleconnection indices utilised in the study the Climate Prediction Center (CPC) utilise the Rotated Principal Component Analysis (RPCA) method used by Barnston and Livezey (1987), but utilizing monthly mean standardized 500-mb height anomalies obtained from the NCEP/NCAR Reanalysis (CDAS) in the analysis region 20°N-90°N. This procedure isolates the primary teleconnection patterns for all months and obtains the index time series.

2.2 Drought identification: The Standardised Precipitation – Evapotranspiration Index

Drought definition makes difficult to conceive a universal drought index. Therefore, there are many indices and different criteria to identify and investigate different types of droughts (Svodoba and Fuchs, 2016). However, it is basically caused by an imbalance between water supply and demand. Therefore, the Standardised Precipitation-Evapotranspiration Index (SPEI) (Vicente-Serrano et al., 2010) was chosen to identify dry conditions in the MLSHD during the period 1980-2017. This index is based on the same methodology of the Standardised Precipitation Index (SPI) (Mckee et al., 1993). However, as an advantage over common precipitation based drought indices (e.g. the SPI) it considers the effects of temperature through the reference evapotranspiration (Eto) in the monthly climatic water balance (D) represented in equation 1. The precipitation (accumulated over a period of time) in the SPEI stands for the water availability, while ETo stands for the atmospheric water demand. Therefore, the SPEI combines the changes the atmospheric evaporative demand with the multiscalar nature of the SPI (Beguería et al., 2014), which allows the assessment of the response of different ecological, hydrological and agricultural systems to drought (Vicente-Serrano et al., 2012). In consequence, it has been applied to a large variety of ecosystems across the world for identifying dry and wet conditions, and evaluating drought recurrence. It was also chosen for this study because the results of Vicente-Serrano et al. (2014) described how drought severity has increased in the past six decades (1954–2014) in natural, regulated, and highly regulated basins of the IP as a consequence of greater atmospheric evaporative demand resulting from temperature rise.

$$D = (P - Eto) \tag{1}$$

Eto is a climatic parameter that expresses the evaporating power of the atmosphere at a specific location and time of the year (Allen et al., 1998). In the absence of meteorological data required for applying the Penman-Monteith equation, which is recommended by the Food and Agriculture Organization (FAO) of the United Nations in the FAO Bulletin 56 (Allen et al., 1998), we used the method proposed by Hargreaves and Samani (1985) based on temperature data to estimate the Eto according to Equation 2:

$$Eto = 0.408 * Ch * Ra * \left(\sqrt{Tx - Tn}\right) + (Tm + 17.8) \quad (2)$$

where Ch = 0.0023; Ra is the extraterrestrial radiation (derived from the latitude and the month of the year), and Tx, Tn and Tm the maximum, minimum and mean temperature respectively. By this method, we do not consider relative humidity and wind speed are also important factors to determine the vapour density above the soil surface and the aerodynamic resistance for vapor transport, permitting more realistic Eto values and consequently drought assessment (Bittelli et al., 2008; Vicente-Serrano et al., 2010; WMO, 2012; Davarzani et al., 2014). However, even though the Penman-Monteith offers a more accurate estimation of reference Eto than the Hargreaves formula (López-Moreno et al., 2009; Tomas-Burguera et al., 2017), results of Vicente-Serrano et al., 2014 showed that Eto in Spain estimated by the Hargreaves-Samani method for the period 1961 – 2011, had the closest agreement with the Eto obtained by the Peaman Monthie method in terms of temporal evolution and magnitude respect other eleven methods. These authors also found high correlations between Eto obtained by both methods in the northwest IP.

The resultant D values in equation 1 were aggregated at different time scales, following the same procedure as the SPI. According to Vicente-Serrano et al., (2010), Beguería et al., 2014 and Vicente-Serrano and Beguería, (2016), for calculating the SPEI at different time scales the most suitable statistical distribution to model the D series is the log-logistic distribution, which is given by equation 3:

$$F(D) = [1 + (\frac{\alpha}{D-\gamma})^{\beta}]^{-1} \quad (3)$$

where α, β, and γ represent the scale, shape, and location parameters that are estimated from the sample D. Finally, the SPEI is obtained as the standardized values of $F(D)$. For the calculation of the SPEI the R package available at http://cran.r-project.org/web/packages/SPEI is utilised. It includes all the recommendations proposed by Beguería et al., (2014).

We avoid considering that any precipitation below the mean constitutes a drought. Therefore, the classification of drought categories for SPI values proposed by Agnew (2000) (Table 1) was utilised in this study. Other authors have also employed this classification for investigating drought in the IP (e.g. Vicente-Serrano et al., 2006; Páscoa et al., 2017). This classification despite to be pre-established is built by probability classes rather than magnitudes of the SPI, and is, therefore, a more rational

approach, with a most noticeable effect at the demarcation of mild and moderate droughts (Agnew, 2000). A drought episode occurs every time the SPEI1 is continuously negative and reaches the value of −0.84 or less. The onset of an episode is the month in which the episode begins, the peak is the month in which the episodes reach the highest negative value of SPEI1 and the end is the last month that SPEI1 is negative. The threshold of -0.84 corresponds to 20% probabilities, whereby a drought is expected to occur once in 5 years, which reduces the incidence of mild meteorological droughts. The duration is computed as the sum of all months from the onset with negative values, and the severity is calculated as the sum of all SPEI values (in absolute values) during the episode.

Table 1. Standardised Precipitation-Evapotranspiration Index (SPEI) classification according to Agnew (2000).

SPEI	Probability	Category
> 1.65	0.05	Extremely humid
> 1.28	0.10	Severely humid
> 0.84	0.20	Moderately humid
> -0.84 and < 0.84	0.60	Normal
< -0.84	0.20	Moderately dry
< -1.28	0.10	Severely dry
< -1.65	0.05	Extremely dry

To identify the principal patterns of drought variability in the MLSHD, an Empirical Orthogonal Functions (EOF) analysis (Preisendorfer 1988; von Storch 1995) was utilised. The EOF analysis is not based on physical principles, however, the technique aims to decompose observed datasets into two components that capture most of the observed variance in space (eigenvalues) and time (eigenvectors), making easier to study the principal modes of variability of the SPEI1 time series for every grid point of the MLSHD. The percentage of the total variance explained by each eigenvector is able to explain most of the spatial drought variance. This method has been extensively used to investigated droughts at global (e.g Dai, 2011) and regional (Wang et al., 2017, 2019) scale.

Trend analysis using the Mann-Kendall Test (Mann, 1945; Kendall, 1975) of Prewhitened Time Series Data in Presence of Serial Correlation using the von Storch (1995) approach was performed. This approach ensures to avoid possible autocorrelation of the series. This method is often used to analyze the trend change of hydrometeorological time series such as precipitation, runoff, drought index, etc. For this analysis the R package 'modifiedmk' (Patakamuri and O'Brien, 2019) is utilised.

2.4 The Standardise Runoff Index (SRI)

The Standardise Runoff Index (SRI) is applied to investigate the occurrence and temporal evolution of hydrological drought in the MLSHD. To computed this index the same approach employed by McKee et al. (1993) for the SPI is here used.

According to these authors, the procedure can be applied to other variables relevant to drought, e.g., streamflow or reservoir contents. Thus, the Gamma distribution is used for fitting monthly runoff data for accumulation periods up to 24 months.

2.4 Weather type classification methodology

Synoptic systems are linked to the dominant climate in any region of the planet. These systems represent the general circulation of the atmosphere through different configurations of variables. For this reason, an objective classification scheme based on the methodology adopted by Trigo and DaCamara (2000) from the Jenkinson and Collison (1977) and Jones et al. (1993) circulation schemes is applied to obtain the dominant circulation weather types (WTs) over the IP. The method uses daily MSLP values obtained from the ERA-Interim reanalysis for the period 1980-2017 on 16 different points over the IP (dots shown in Figure 1) in order to build a set of indices associated with the direction and vorticity of the geostrophic flow, namely total shear vorticity (Z), southerly shear vorticity (ZS), westerly shear vorticity (ZW), total flow (F), southerly flow (SF), and westerly flow (WF). The area used to compute WTs is the same as used by Ramos et al. (2014) and it comprises in longitude from 20ºW to 10ºE and in latitude from 30 to 50ºN. The regional indices are computed as follows (Equations 3 to 8) according to the procedure described in Ramos et al. (2014) and Trigo and DaCamara (2000) taking into account the 16 points named as p_x (x going from 1 to 16 according to the number of the point represented in Figure 1).

$$SF = 1.305[0.25(p_5 + 2 \times p_9 + p_{13}) - 0.25(p_4 + 2 \times p_8 + p_{12})] \quad (4)$$

$$WF = [0.5(p_{12} + p_{13}) - 0.5(p_4 + p_5)] \quad (5)$$

$$ZS = 0.85 \times [0.25(p_6 + 2 \times p_{10} + p_{14}) - 0.25(p_5 + 2 \times p_9 + p_{13}) - 0.25 \times (p_4 + 2 \times p_8 + p_{12}) + 0.25(p_3 + 2 \times p_7 + p_{11})] \quad (6)$$

$$ZW = 1.12 \times [0.5 \times (p_{15} + p_{16}) - 0.5 \times (p_8 + p_9)] - 0.91 \times [0.5 \times (p_8 + p_9) - 0.5 \times (p_1 + p_2)] \quad (7)$$

$$F = (SF^2 + WF^2)^{1/2} \quad (8)$$

$$Z = ZS + ZW \quad (9)$$

Following this approach, 26 WTs are initially identified (10 pure, 8 anticyclonic hybrids and 8 cyclonic hybrids). Pure directional WTs (Northeastern (NE), Eastern (E), Southeastern (SE), Northwestern (NW), Western (W), Southwestern (SW), North (N), South (S)) are those showing $|Z| < F$ with the direction defined by $\tan^{-1}$ (WF/SF) (180° added if WF is positive). If $|Z| > 2F$ then the circulation would be considered cyclonic (C) (if $Z > 0$) or anticyclonic (A) (if $Z < 0$). As not all the circulation patterns can be associated with a pure (directional/cyclonic/anticyclonic) type, 16 hybrid circulations are defined as a combination of A and C circulation with directional WTs. In this case $F < |Z| < 2F$. As in other previous studies, we distributed the few cases (<2%) with unclassified situations among the 26 classes. The unclassified situations occur when the module of the total shear vorticity (Z) is less than the standard deviation of Z/2 and simultaneously the total flow (F) is less than the square root of the sum of squared westerly and southerly flows. Following Trigo and DaCamara (2000) in the frequency

computation, the 26 WTs are regrouped in the 10 "pure" ones – thus each of the 16 hybrid types count equally as a half occurrence to each of their corresponding pure directional and cyclonic/anticyclonic types (e.g. one case of CNW is included as 0.5 in C and 0.5 in NW).

The methodology here described is able to daily identify the dominat weather pattern (from the WT listed above) over the area of study. From this daily information and in order to study the WTs influence on the monthly SPEI series, the monthly frequency of occurrence for every pure WT is computed for the period 1980-2017.

2.5 Wavelet coherence analysis

Wavelet coherence (WC) analysis is used to identify which frequency bands within two time series are co-varying (Torrence and Webster, 1999). This definition is similar to that of a traditional cross correlation, and the WC can be considered as a localised correlation coefficient in time-frequency space (Torrence and Compo, 1998; Grinsted et al., 2004). For this assessment, the SPEI at the temporal scale of 1 month (SPEI1) and six monthly series of teleconnection patterns, namely the BEST, WeMO, NAO, AO, EA, and SCAND were utilised by initially applying Equation 10, as follows:

$$R_n^2(S) = \frac{\left|S\left(s^{-1}W_n^{XY}(s)\right)\right|^2}{S\left(s^{-1}\left|W_n^X(s)\right|^2\right) * S\left(s^{-1}\left|W_n^Y(s)\right|^2\right)} \quad (10)$$

where S is a smoothing operator and XY are the two series. The WC ranges from 0 to 1; if the value is closer to 1, then the correlation between the two series is higher. The cross-wavelet coherence analysis was performed using the "wtc" function throught the biwavelet R package (https://CRAN.R-project.org/package=biwavelet). The WC 5% significance level is determined using Monte Carlo generated noise 1000 randomizations. An advantage of WC over the classical cross-correlation analysis is that the phase relationship is calculated such that the degree to which two time series are positively or negatively related can be measured as both a function of time and period (Shulte et al., 2016).

3. Results and discussion

3.1 Drought conditions

The northwest IP is a homogeneous region in terms of the total P variance over the IP (Rodriguez-Puebla et al., 1998; Muñoz-Díaz and Rodrigo, 2005), and consequently, the influence of droughts (Russo et al., 2015). Such regions can be delineated using precipitation datasets and conventional approaches such as principal components clustering procedures, indices (Mallants and Feyen, 1990; Awan et al., 2015; Bharath, and Srinivas, 2015). As our aim is to investigate meteorological droughts in the MLSHD, it was primarly performed an EOF analysis using the SPEI at one month temporal scale (SPEI1). At

this time scale, the SPEI is the best indicator of the monthly water balance of the region. The results in Figure 3 reveal the spatial characteristics of the first three leading EOF modes, which explain 97.8% of the total spatial variability of the SPEI1 in the MLSHD. Because the spatial patterns of the remaining EOFs explain very low percentages they are not shown. In particular, the EOF1 (93%) is characterised by all negative values, indicating that dry or wet conditions in the MLSHD manifest themselves homogeneously throughout its entire extension. The spatial coefficients of EOF2 separate the eastern high lands from the north and west of the MLSHD, while the EOF3 reveals the north-south spatial differences. However, both explain just 2.6% and 2.2% respectively. According to these findings, the MLSHD can be considered a homogeneus hydroclimate region.

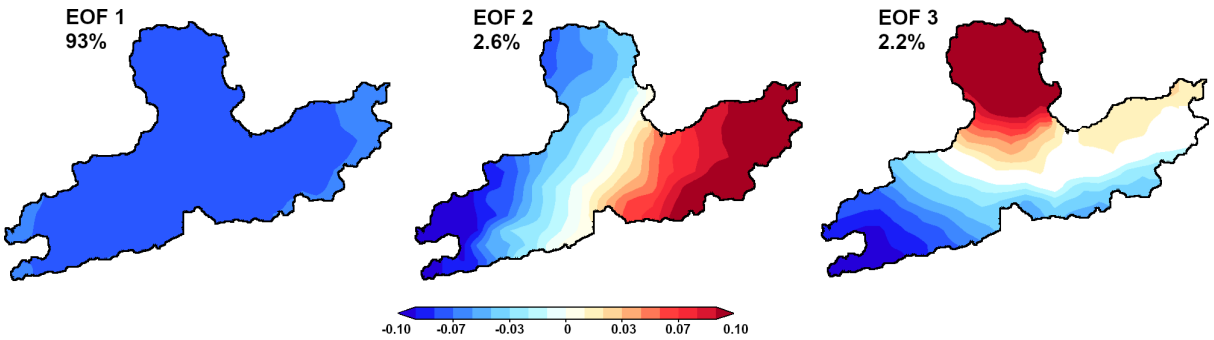

Figure 3. The first three leading EOF modes of the SPEI1 for the MLSHD. Period 1980 – 2017.

Figure 4a shows the temporal evolution of the SPEI1 computed for the MLSHD during 1980–2017. The high variability of the series made it difficult to identify the most extensive (in terms of duration) and intense (in terms of severity) periods affected by dry conditions. However, this prevailed in periods such as 1989–1992, 2004–2007, and 2015–2017, which is in agreement with results obtained by other authors for the north western IP through different indices (e.g., Garcia-Herrera, 2007; Andrade and Pereira, 2015; Spinioni et al., 2016; Ojeda et al., 2019). At this time scale, the negative values of the SPEI are primarily related to meteorological drought, which is unable to diagnose the agricultural, hydrological, and socioeconomic types of drought. However, meteorological droughts can be perceived as the initial cause of further types of droughts, since these are triggered by the deficit of P combined with high temperatures and significant Eto. The identification of meteorological drought episodes affecting the IP has been a topic of research during the last years (e.g. Lana et al., 2006; Lorenzo-La Cruz et al., 2013; Páscoa et al., 2017; González-Hidalgo et al., 2018). As a drought episode is considered to occur every time the SPEI1 is continuously negative and reaches the value of −0.84 or less; this threshold is identified by the black dashed line in Figure 4a. The onset, termination, and duration of these episodes are shown in Figure 4b. According to the visual analysis, the frequency of long episodes increased after 2003.

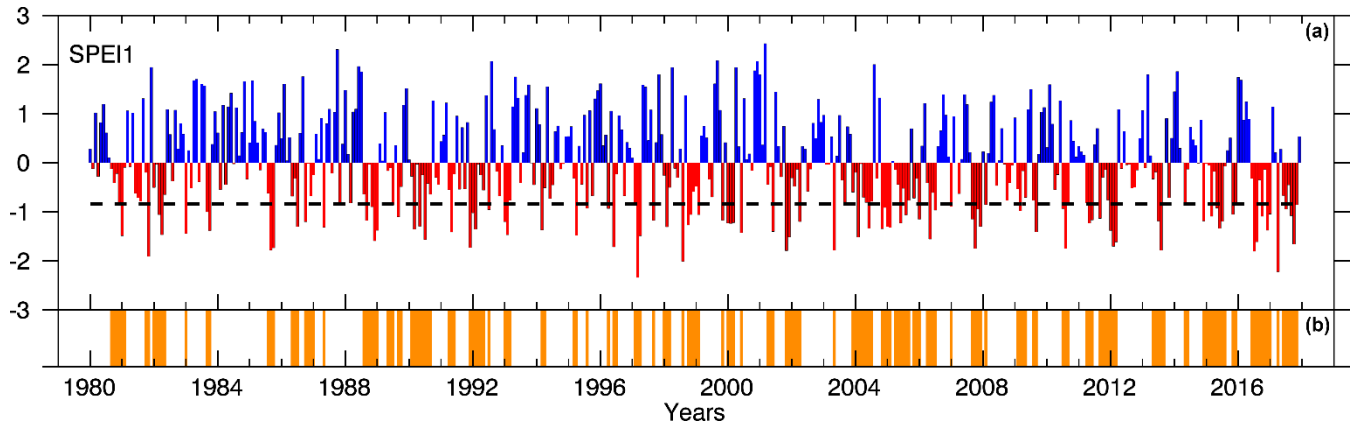

Figure 4. Wet (blue bars) and dry (red bars) conditions according to the Standardised Precipitation-Evapotranspiration Index at the 1 month temporal scale (SPEI1) (a), and dry episodes (orange bars) (b) during 1980–2017.

Results of Sáez de Cámara et al. (2015) note noteworthy tendency toward less wet days with a decreasing trend in the average precipitation per wet day for western and central north IP. A tendency analysis for the period of study reveals a small negative trend in the series of the SPEI1 (statistically significant); an increase in the dureation of the episodes (not statistically significant) and a small increase on the severity of these episodes (statistically significant) (Table 2). Vicente-Serrano et al. (2011) also found that mean duration of drought episodes in the north western IP increased by approximately 1 month in the last 30 years of 1930–2006 (difference not statistically significant) as a consequence of the increase in potential evapotranspiration. For the number of drought episodes the trend is not statistically significant.

Table 2. Trend analysis of the 1-month Standardised Precipitation-Evapotranspiration Index (SPEI1) series and number of episodes that start per year, their duration, severity. The slope represents the trend. Statistically significant trends are marked with an asterisk. Significance is calculated using the t-distribution of the test statistic, and the trend is considered significant when $p < 0.05$.

	Slope	**Units**	***p* value**
SPEI1	-0.0007*	$year^{-1}$	0.04
Number of Episodes	0.000	episodes/year	0.59
Duration	0.031	month/year	0.09
Severity	0.028*	$year^{-1}$	0.04

Extreme drought events can disrupt food production systems and thus be a significant natural trigger for famine (Wilhite, 2000) and for the MLSHD can directly affect the hydroelectric production. The top 10 driest episodes in the period under study according to their severity are shown in Table 3. This selection was made to develop further analysis based on extreme meteorological dry conditions. In this table are also represented the onset, peak, end, peak value, and duration and severity of each episode.

Table 3. The 10 most severe drought episodes that affected the Miño-Limia-Sil Hydrographic Demarcation from 1980 to 2017 organised based on their severity from higher to lower. The onset (first month of the episode), peak (lower SPEI1 value during the episode), termination (last episode month), and duration (number of months from the onset to the termination) are shown.

Episode	Onset	Peak	End	Peak value	Duration	Severity
E1	Jun/2016	Jul/2016	Jan/2017	-1.80	8	7.7
E2	Sep/2011	Feb/2012	Mar/2012	-1.70	7	7.0
E3	Dec/2014	Jun/2015	Aug/2015	-1.34	9	6.1
E4	Dec/2003	Feb/2004	Jul/2004	-1.52	8	6.0
E5	Feb/1990	Jul/1990	Sep/1990	-1.56	8	5.8
E6	Aug/1988	Dec/1988	Jan/1989	-1.60	6	5.7
E7	Jun/2017	Oct/2017	Nov/2017	-1.66	6	5.6
E8	Nov/2001	Dec/2001	Apr/2002	-1.80	6	5.4
E9	Sep/2007	Oct/2007	Dec/2007	-1.74	4	5.1
E10	Dec/1991	Dec/1991	May/1992	-1.72	6	4.9

Through SPEI it is not possible to know independently the role of the P or ETo in the occurrence and magnitude of the drought. That is why in the Figure 5 the accumulated P during each drought episode (solid lines) listed in table 3 are illustrated, as well as the monthly accumulated percentiles 5 (P05), 10 (P10) and 25 (P25) of P for the study period (1980 – 2017) (discontinued lines). The order of the episodes in this figure is determined by the month of their beginning. Accumulated P during June and July of the E1 was between the P05 and P10, but later was between p10 and p25. In the E7 the accumulated P was between p10 and p25 from June to August, and afterword, from September to November it was even drier (between P05 and P10). For all 10 episodes the accumulated P was never above the P25, confirming the precipitation deficit.

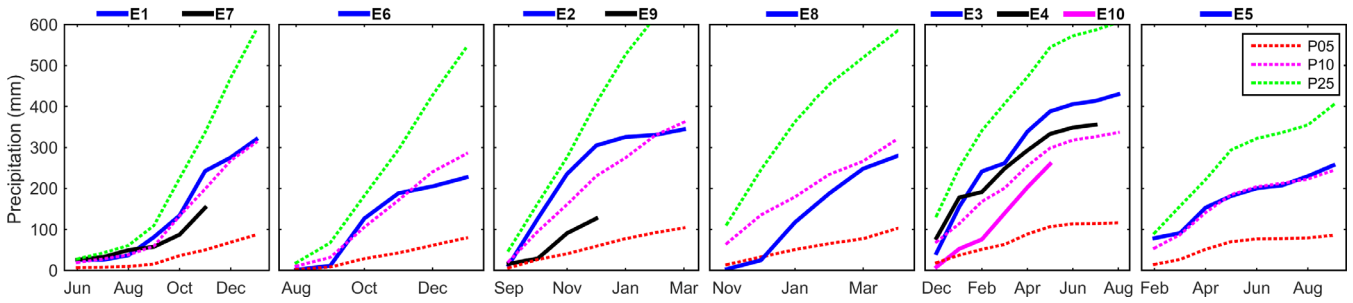

Figure 5. Accumulated P during each drought episode listed in Table 3 (solid lines), and the montly accumulated percentiles 5 (P05), 10 (P10) and 25 (P25) of P (discontinued lines), but considering the whole study period (1980 – 2017).

The spatial variability of droughts is a concern for decision making of water resources policy and management. In Figure 6 six annual leading modes of EOF are shown, which explain 94% of the total spatial variability of the SPEI1 for those months when the SPEI $\leq$ -0.84 in the MLSHD (represented in Figure 4b). These represent potential physical modes of drought variability in the MLSHD. The first eigenvector (EOF1) explains 61%. This pattern is very homogeneous, with close negative

values in all the MLSHD, indicating a great spatial similarity of the main drought pattern and the predominant influence of large-scale factors. Although, a visual analysis of EOF1 also shows a small longitudinal difference with more intense negative values on the eastern part of the MLSHD (farther from the coast). As expected, the characteristics of the following EOFs represented in Figure 6 show major spatial differences. The EOF2 explains 17% of the total drought variability. In it, the major differences are observed between the eastern part of the region, where prevails positive values, and the rest of the territory with negative values, indicating different spatial drought magnitudes. In Figure 1 can be observed that the eastern of the MLSHD is characterised by major elevation. Therefore, spatial drought variability in this pattern can be explained by orographic differences. The EOF3 explains 9% of spatial drought characteristics, which are determined by a gradient from positive to negative values from the coastal zone to the northeast respectively. The remaining EOFs show a greater spatial variability and lower percentages of explained variance.

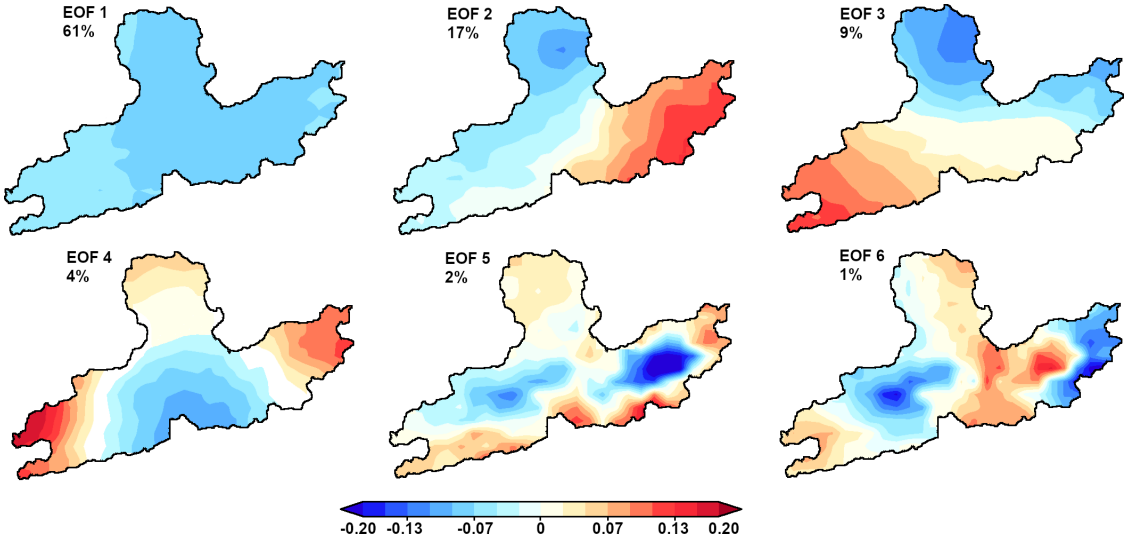

Figure 6. Six leading modes of EOF for the SPEI1values ≤ -0.84.

3.2 Relationship between the circulation weather type classification and drought conditions

The MSLP fields and anomalies for the 10 pure WTs responsible for the major variability in atmospheric circulation over the IP are shown in Figure 7. These anomaly composites are obtained after removing the respective grand means computed for the period 1981-2010. These patterns (obtained using the same methodology) have previously been used to investigate the relationships between the atmospheric circulation and precipitation variability (e.g. Cortesi et al., 2014; Ramos et al., 2014) or drought conditions in the IP (e.g. Russo et al., 2015). Here we aim to determine the association of large-scale atmospheric circulation over the IP with drought conditions that affected the MLSHD during 1980-2017. The reddish (blueish) isolines in Figure 6 identify the higher (lower) values in the MSLP absolute fields and the positive (negative) values of MSLP anomalies. The NE configuration (Figure 7a) is characterised by a transition from a strong high-pressure region over the eastern Atlantic

Ocean extending to the northwestern Iberia and the MLSHD, and lower pressures over Africa. The anomaly field (Figure 6b) shows that this high pressure centre is displaced towards northeast, to the west of the UK. In the E and SE configurations (Figure 7a), the high-pressure system is shifted northwards and centred over the Cantabrian Sea and the Celtic Sea in the E circulation, while in the SE circulation it is centred over France and the southern UK. The anomaly fields (E and SE; Figure 4b) show an intensification of 8 hPa to10 hPa of these high pressure system. In the S pattern, higher pressure values occur over central Europe and lower pressure values (1010 hPa) over the Northeast Atlantic (Figure 7a) which become up to 8-10 hPa lower (Figure 7b). In the SW WT high-pressure values are limited to the most southern areas in the North Atlantic and a well-developed low-pressure system (1000 hPa) is located over Northeast Atlantic (Figure 7a). The anomaly fields show an intensification of these systems to the northwest region of Iberia– up to -20 hPa (Figure 7b). In the W and NW configurations the low-pressure systems are shifted northwards and north-eastwards towards the UK, respectively, while the Azores high establishes (Figure 7a). The corresponding anomaly fields illustrate the intensification of these low-pressure systems (Figure 4b). The high-pressure systems identified in the case of the NW configuration are more intense in the N WT (Figure 7a) and the anomaly shows a northward displacement of these systems, covering all the Atlantic regions, while low-pressure systems are more developed over the Gulf of Lion, in the Mediterranean (Figure 7b). Finally, the C WT represents low relative pressures located over the western IP (Figure 7a) which intensify, while positive anomalies develop to the northern regions, west of the UK (Figure 7b); the opposite occurs for the A configuration which represents an intense Azores high, extended towards Europe (Figure 7a). The anomaly shows that under these conditions the high-pressure systems intensify over the IP and southwest Europe (Figure 7b).

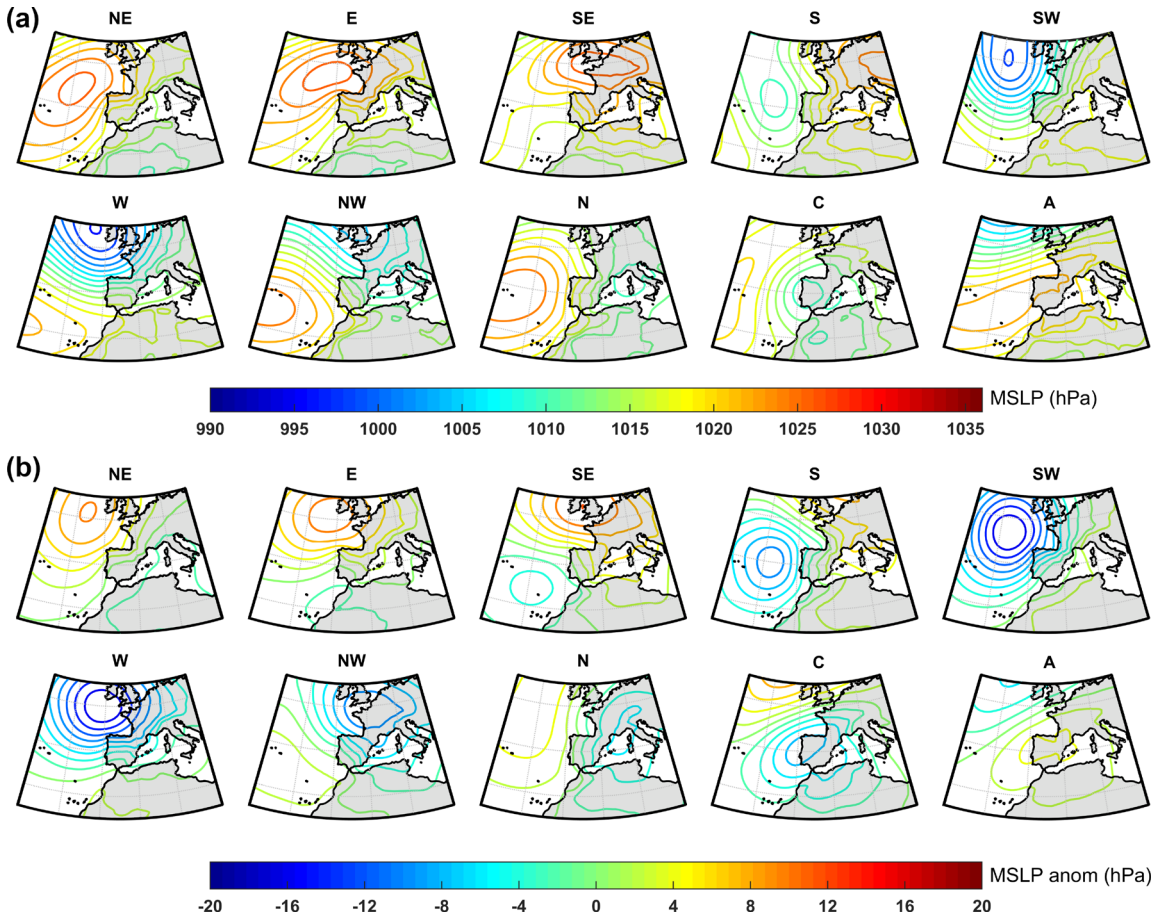

Figure 7. Mean sea level pressure (MSLP) fields (a) and anomaly (b) fields' configuration of the 10 pure weather types (WTs) for the period 1980-2017. The contour interval is 2 hPa.

The correlations between the monthly percentage values of the occurrence of each of the pure WTs with the SPEI1 time series are shown in Figure 8. WTs and SPEI1 time series were de-trended before correlation computation. Highlight the significant positive correlations found with SW, W, and NW WTs, in agreement with the results of Russo et al. (2015), but for the whole northwestern IP. Indeed, air masses from the SW, W, NW and C usually associated to inbound baroclinic structures, Atlantic storms and Atmospheric Rivers (Eiras-Barca et al. 2018) carry moisture from the Bay of Biscay (BB) and the Tropical and Subtropical North Atlantic corridor to the MLSHD, both principal sources for precipitation over the Galicia and northern Portugal (Drumond et al., 2011). The C WT appears to be mostly positively correlated with SPEI1; however, for almost all months the correlations are not statistically significant. The extratropical cyclones and the associated synoptic-scale fronts reaching the IP during winter months and early spring normally produce large accumulated rainfall and play an important role on the hydrological cycle in northern Portugal and Galicia (Paredes et al., 2006; Añel et al., 2012; Hénin et al., 2019).

Contrastingly, the atmospheric circulation associated with NE, E, and SE WTs is negatively correlated with the SPEI1 time series in all months, thereby suggesting that air masses associated with these are directly related to the dry conditions at the MLSHD. Negative correlations between the SPEI1 and the A WT mostly occur during winter months WT; however, these are lower and not significant during several months. On the contrary, the correlations between SPEI1 and C are mostly positive, but mostly not statistically significant. Finally, as expected, monthly correlations between the atmospheric circulation associated with N and S WTs with the SPEI1 have generally opposite sign values, in addition to being very low and not statistically significant. Trigo et al. (2004) associated the mean annual and seasonal rainfall decrease across the IP during the second half of the XX century to the lost of the high-rainfall circulation types (cyclonic) and with the increase of the low-rainfall types (anticyclonic). However, a trend analysis for the period 1980-2017 (not shown) revealed no statistically significant trend in the series of any WT.

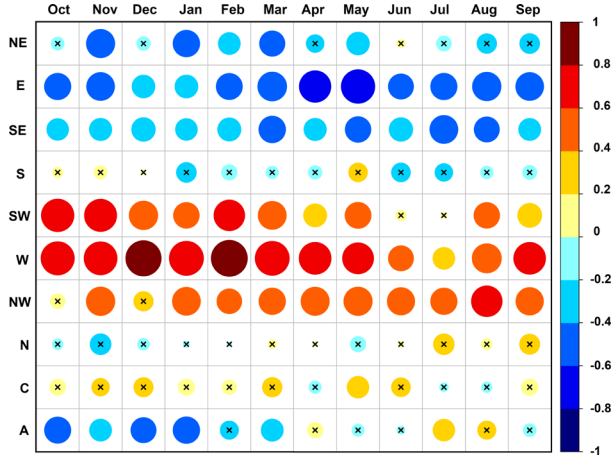

Figure 8. Correlations between detrended series of 1 month Standardised Precipitation-Evapotranspiration Index and the monthly percentage of occurrence of each of the pure weather types for 1980–2017. The size of the circles is proportional to the correlation values. The x's inside the circles represent not statistical significant correlations at $p < 0.05$.

The spatial patterns of correlations between detrended series of the SPEI1 and the climatic teleconnections indices appear in Figure 9. In most of the patterns no different signs of the correlation are observed, coinciding with the sign of the correlation shown in figure 8. This confirms that there is a homogeneous influence of climatic variability modes on the variability of dry/wet conditions in MLSHD according to the SPEI1. However, it is observed local variations of the correlation. For example, the spatial correlations of the SPEI1 with the W and E WTs show a west-east gradient from highest to lowest values. The correlations are statistically significant throughout the MLSHD only for SE, E, SW, W and NW WTs.

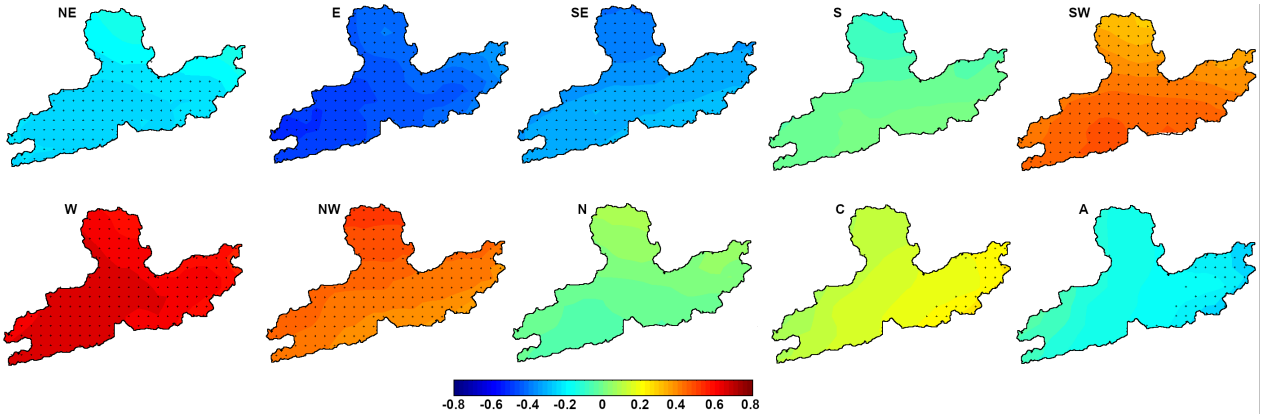

Figure 9. Spatial correlations between detrended grid series of 1 month Standardised Precipitation-Evapotranspiration Index at a resolution of 0.1° in longitude and latitude, and detrended monthly percentage of occurrence of each of the pure weather types for 1980–2017. The symbols in every correlation map denote statistical significant correlations at $p < 0.05$.

In order to understand how distinct WTs might affect drought severity in the MLSHD, Figure 10 shows the monthly frequency (expressed in percentage) of each WT under different drought categories (moderately dry, severely dry, and extremely dry) according to the SPEI classification shown in Table 1. Those Octobers under moderately dry conditions are associated with the prevalence of A, E, and C WTs. Octobers affected by severely dry conditions are associated with a major percentage of A circulation, but for those under extreme drought conditions seems that E circulation highly increased with respect to previous drought categories, while there was a slight decrease in the frequency of A circulation. For those Novembers affected by moderate, severe, and extreme drought conditions the most frequent WT was the A circulation, which imposes an atmospheric flux from the north. For severely and extremely dry Decembers the frequency of WTs change with respect to those of previous months, and an increase in the percentage of SE circulation is observed. Januaries under moderate and severe drought conditions are characterised by a major percentage of atmospheric conditions governed by the A pattern. In February, the percentage of occurrence of A WT decrease when drought severity increase, while highlight the E increase for severely drought months and the NE increases for extreme drought months. For those March under drought conditions the most frequent patterns are the A, E, NE. The frequency of WTs for those April affected by drought conditions is remarkably different respect already described for previous months. In this month the E and SE WTs are directly related to drought severity increase. In the following months (May to September) affected by different drought categories, the combination of NE, E and A WTs is the most frequent according to the percentage observed in the figure.

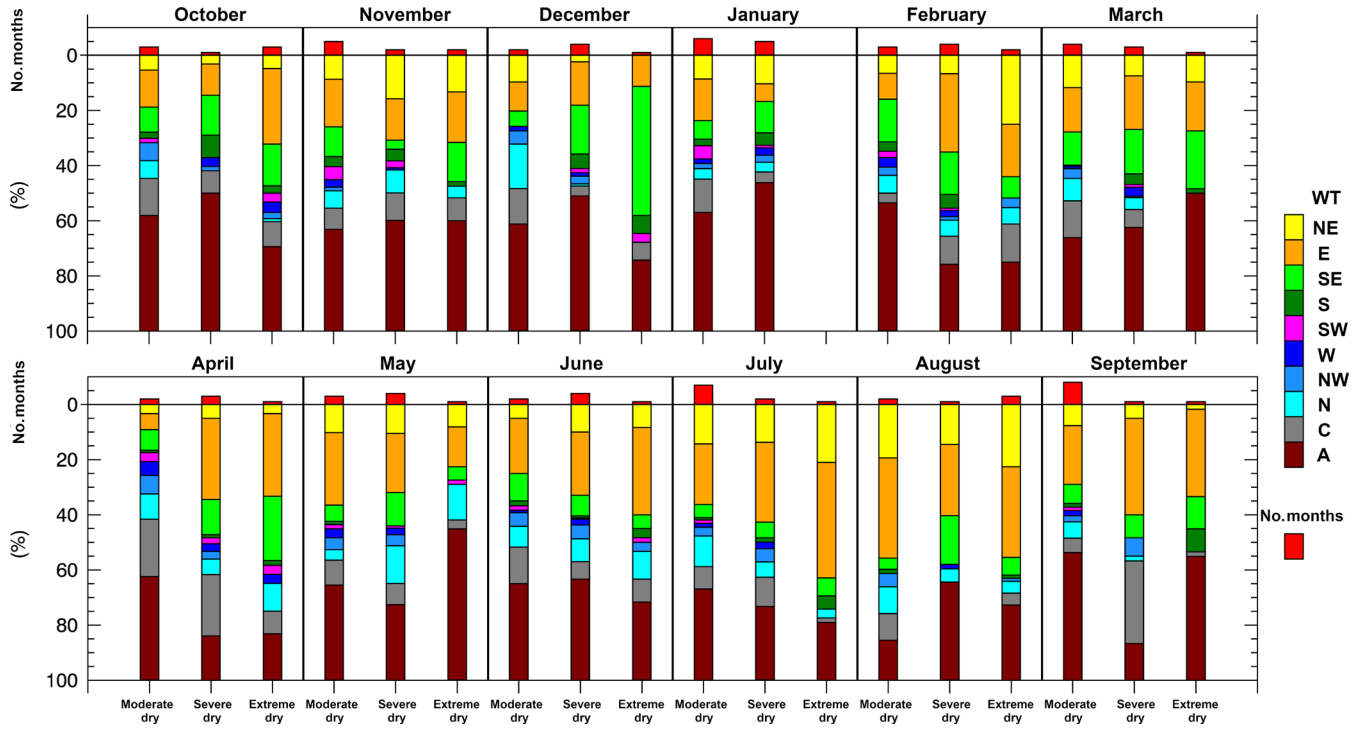

Figure 10. Monthly percentage of occurrence for every WT associated with moderate, severe and extremely dry conditions. The red bars represent the number of months the MLSHD was affected by severe and extremely dry conditions.

The most severe drought episodes are also investigated. Figure 11 shows the accumulated SPEI1 (red line) during the 10 most severe drought episodes listed in Table 3. The coloured areas in this figure represent the WTs that occurred for every day of the episode. WTs are grouped taking into account the monthly correlation results presented in Figure 8. A visual analysis allows to conclude that along with the temporal evolution of all episodes the most frequent WTs are the eastern (NE-E-SE) (yellow colour) and A (orange colour). In agreement with previous results above described, for most of the episodes the eastern circulation seems to be specially related to the drought intensification, being the most common WT during the peak month of each event. Western circulation patterns appear randomly during the episodes. In the last days of E1, E5 and E6 are observed SW, W, and NW WTs, while in the last days of E2, E3, and E7 are observed the C.

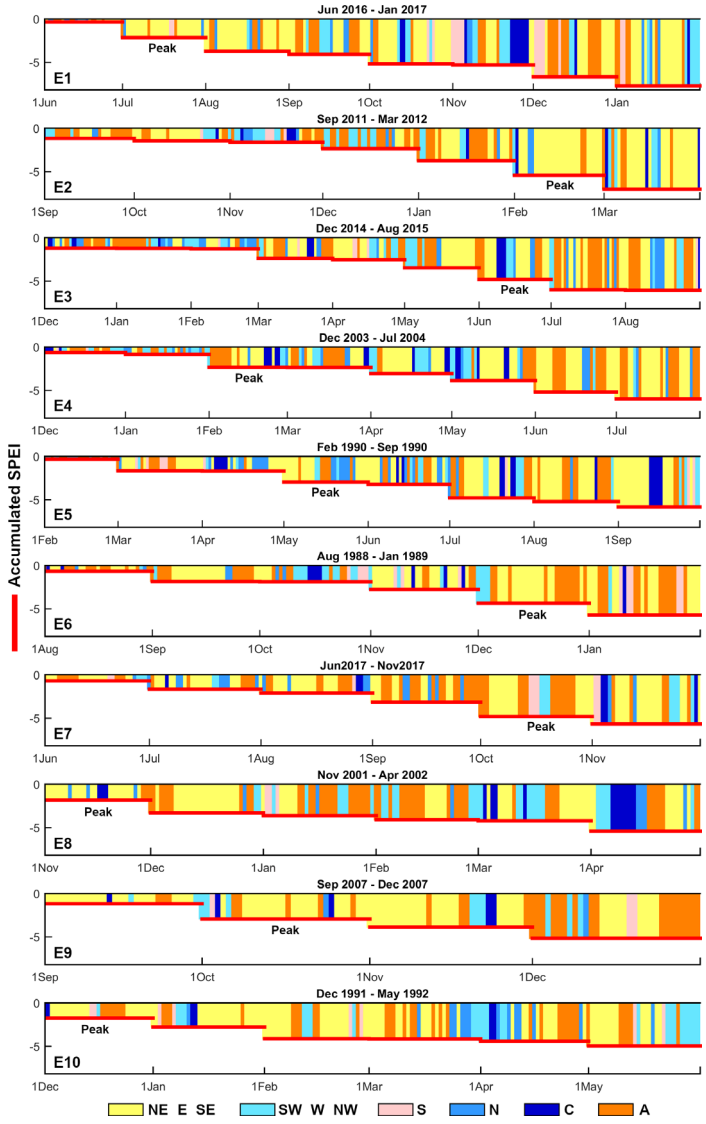

Figure 11. Accumulated SPEI1 (red line) and grouped WTs during the 10 most severe drought episodes listed in Table 3.

The anomaly in the percentage of occurrence of every pure WT during the 10 most severe episodes is shown in Figure 12. The anomaly has been calculated for the complete duration of each drought episode, and referred to the 1980–2017 mean value for the same months. The eastern (NE, E, SE), A, and S WTs experiment mostly positive anomalies, in accordance with the results described above for Figure 10. Conversely, in most of the episodes the anomaly of western circulations (NW, W, SW), N and C, decrease. The largest negatives anomalies appear for the W WT, which falls as an average between 2.5% and 5.7%. Similar results are observed when the total number of severe events were considered (Figure S1).

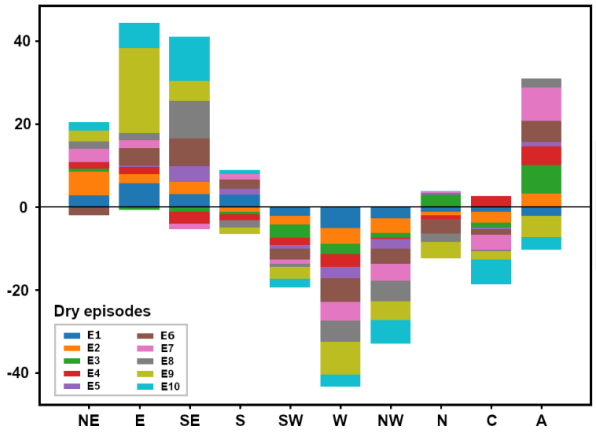

Figure 12. The anomaly in the percentage of each weather type associated with the 10 most severe drought episodes showed in Table 3.

According to Drumond et al. (2011), the nature of rainfall variability over the north of Portugal and Galicia is associated with the moisture transport from two dominant moisture sources, namely the Bay of Biscay and the Tropical and Subtropical North Atlantic corridor; the latter extends from the Gulf of Mexico to Africa from 16°N to 40°N. Figure 13 shows the anomaly of the VIMF and its divergence for the onset, peak, and termination of drought episodes listed in Table 3. The E1 was the driest, and was associated with anticyclonic circulation of the VIMF with centre located to the southwest of the MLSHD. This centre moved to the north in the peak of the episode, imposing moisture flux anomalies from the northeast. This is supported by prevailing A and NE WTs, which decreased in percentage when drought disappeared (February 2017), in accordance with the major frequency of C, W, and SW circulation and negative anomalies of the VIMF divergence (favouring the convergence). The E2 began in September 2012. For this month are observed intense positive anomalies of the VIMF divergence over the MLSHD, a dynamic limitation for the occurrence of precipitation. A and NE WTs were the most frequent this month. The peak of this episode occurred in February 2012, when intense anticyclonic anomalies of the VIMF with centre near the southwest of Ireland dominate the North Atlantic sector. In accordance, NE and E circulations were the most frequent over the IP. Drought conditions disappeared (in April 2012), when negative anomalies of the VIMF divergence in association with cyclonic circulation anomalies of the VIMF with the centre located over England affected the MLSHD. Correspondingly, the most frequent circulation patterns this month were C and NW. The third and fourth driest episodes began in December of 2014 and 2003, respectively. In both months, the most prominent circulation patterns were associated with A WT. Anticyclonic anomalies of the VIMF with centre over the North Atlantic affected the MLSHD; these anomalies were more intense in December 2014, when positive anomalies of the VIMF divergence covered almost all the IP. The peak of E3 occurred in July 2015 with intense VIMF anomalies from the Atlantic Ocean that reached the northern portion of the IP; however, over the MLSHD, both negative and positive VIMF divergence anomalies are observed. The last month of E3 was August 2015,

because the SPEI changed to a positive value in September 2015 owing to negative anomalies of the VIMF divergence over the north western IP and the influence of anomalies VIMF anomalies reaching the MLSHD from the northwest, in accordance with an increase in the percentage of the W WT with respect to that in the previous stage of the episode. In the peak of E4 are observed positive anomalies of VIMF divergence over the MLSHD. This episode ended when the anomalies on the moisture flux from the west favoured the occurrence of convergence, despite the fact that the most frequent WT was A, followed by W. E5 began in February 1990. In this month the VIMF anomalies over the IP show an intense anticyclonic circulation accompanied by positive divergence anomalies over all the IP, and consequently, a high frequency of A circulation. In the peak is not clear the pattern of VIMF divergences, but one month after the termination the SPEI1 became positive due to negative anomalies of the VIMF divergence and enhanced moisture flux reaching the MLSHD from the northwest.

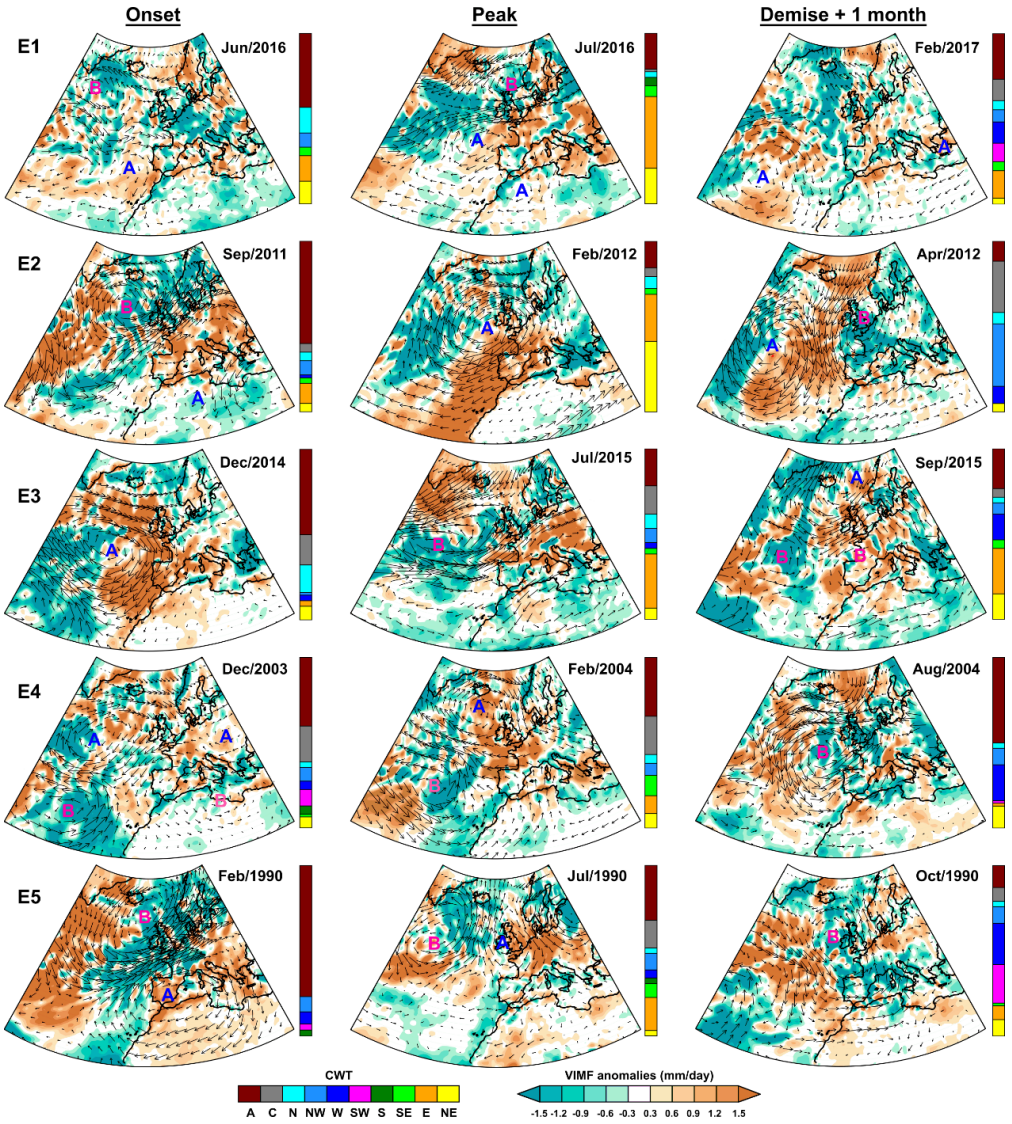

Figure 13. The monthly anomaly of the VIMF (in arrows) and its divergence (shaded) during 1980–2017 for the onset, peak, and 1 month after the termination of each of the ten most severe drought episodes (Es) shown in Table 3. Anticyclonic (cyclonic) centres of the VIMF anomalies circulations are represented as A (B). Vertical bars show the monthly percentage of each pure weather type (WT).

In August 1988 the VIMF anomalies in the onset of E6 are characterised by an anticyclonic circulation centre to the southwest of the MLSHD, and cyclonic circulation in the northwest, which were both over the Atlantic Ocean (Figure 13 continued) and enforced VIMF anomalies reaching the MLSHD from the west. Nevertheless, the VIMF divergence anomalies show prevailing divergence conditions. That is, the MLSHD can receive air masses from the west, which, as already described, are associated with the increase in wet conditions, but dynamic atmospheric conditions can inhibit the occurrence of precipitation. In the peak of this episode (December 1988) a centre of anticyclonic circulation of the VIMF is observed in the north Atlantic Ocean to

the northwest of the IP produced an intense divergence of the VIMF over the MLSHD. Predominant frequency of the A and E WTs are also observed this month. This episode ended when VIMF anomalies reached the MLSHD from the northwest, in combination with negative anomalies of the VIMF divergence over the MLSHD. In the onset of E7, as well as in E6, a centre of anomalous cyclonic circulation of the VIMF is observed in the north Atlantic Ocean to the northwest of Ireland. This situation is totally different at the peak of the episode (Oct/2007). In this month anticyclonic circulation of the VIMF with the centre located to the northwest and near the MLSHD imposed strong divergence of the VIMF over the MLSHD, while prevailing frequency of A and E WTs occurred. In December 2017 this centre was located further west, the VIMF divergence anomalies became negative over the MLSHD, and the SPEI1 turn out to be positive. In E8, the onset (Nov/2001) coincided with the peak of the episode. This month was characterised by the prevalence of E and NE WTs and positive anomalies of the VIMF divergence associated with strong anomalous anticyclonic circulation of the VIMF over the North Atlantic Ocean. This episode ended in April 2002 owing to a positive SPEI1 value in May 2002. A small area of negative VIMF anomalies over the MLSHD is observed this month. As well as in the previous episodes, the onset of E9 and E10 is characterised by anticyclonic anomalies of the VIMF with the centre located to the northwest of the MLSHD over the Atlantic Ocean. Strong VIMF divergence is observed over the MLSHD in the peak of E9 and the onset of E10. The onset and peak of E10 coincided. The VIMF anomaly pattern this month (Dec/1991) is characterised by anticyclonic circulation with centre located in the North Atlantic Ocean to the northwest of the MLSHD near Ireland. This pattern is very similar for the peak of the E9, E2, E5, E6, and E7. Both episodes E9 and E10 ended owing to negative anomalies of the VIMF divergence (specially in E10).

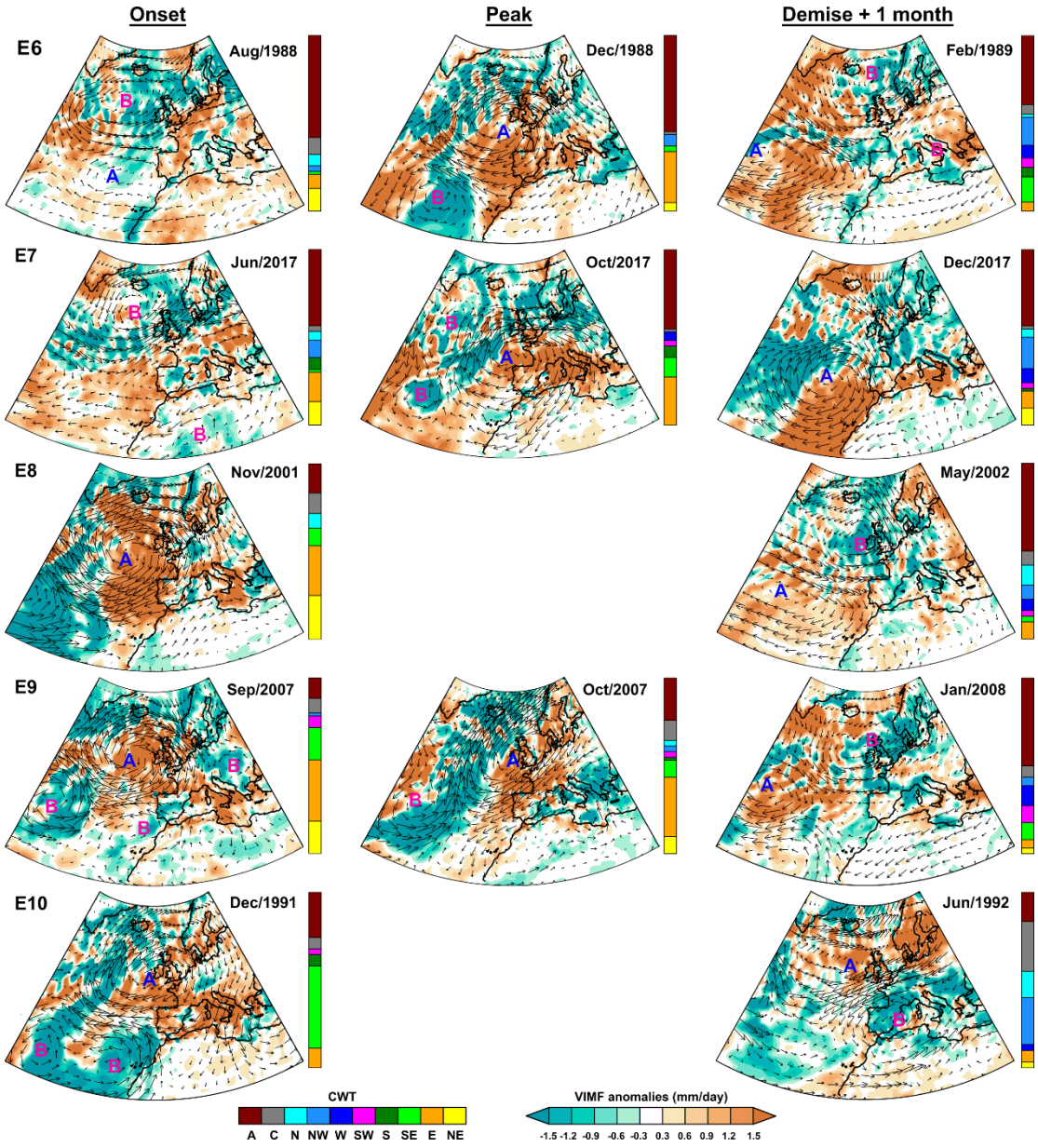

Figure 13. Continued.

3.3 Relationship between drought and modes of climate variability

Figure 14a shows the correlation between the BEST, NAO, EA, AO, SCAND and WeMOi series with SPEI1 to 24. This analysis helps to determine any causal effect between atmospheric and oceanic teleconnection patterns and dry and wet conditions in the MLSHD. The results reveal a major link between the SCAND (positive correlation) and AO (negative

correlation), particularly at short temporal scales of the SPEI (1 to 4 months). The SCAND pattern (initially referred to as the Eurasia-1 by Barnston and Livezey (1987)) in its positive phase is characterised by positive height anomalies over Scandinavia and western Russia, but weaker centres of the opposite sign over the south and western Europe. The negative phase is the opposite. Results of Rodriguez-Puebla et al., (1998) show heterogeneous spatial correlation between the SCAND index and the annual precipitation over the IP; however, they confirmed that annual precipitation variability in the northwestern of IP is related to the SCAND December pattern. On the contrary, the AO ranges from positive to negative values depending on the pressure anomalies in the Arctic region (Thompson and Wallace, 1998). A band of strong winds circulating around the North Pole associated to the positive phase of the AO keep colder air within the polar region, and correspond to a deepening of the Azores High and the strengthening of the polar and subtropical jets over the Euro-Atlantic region (Ambaum et al., 2001). In the negative phase, this ring becomes weaker, thereby allowing the southwards penetration of Arctic air masses and an increase in the magnitude of the total eddy energy fluxes into the Euro-Atlantic region (Rivière and Drouard, 2015), which clearly affects the hydroclimatic conditions in the northwest IP (deCastro et al., 2006) and explains the negative correlations obtained with the SPEI. According to Wanner et al. (2001), the AO is similar to the NAO in many aspects. The negative phase of the NAO is associated with the weakness of the Azores High, and a southwards position in the storm tracks, thereby resulting in wet conditions over the IP (Trigo et al., 2002). The correlations in figure 14a demonstrate that both influence the water balance (through the SPEI1) in the MLSHD on the same SPEI temporal scales. Although, the correlations with AO are major, indicating that AO index may be better than NAO to explain the atmospheric influence on dry/wet conditions in the MLSHD. Nevertheless, the NAO index has been also traditionally defined as the normalized pressure difference between a station on the Azores and one on Iceland (Hurrell, 1995; Jones et al., 1997) and therefore the correlations with the SPEI could be also different.

The correlations between the SPEI with the BEST index are positive, but very low (< 0.2) and not significant; these became negative when correlations were made with SPEI values computed from the past 6 months to 24 months, but were also not statistically significant (Figure 14a). ENSO is namely the strongest ocean-atmosphere coupling phenomenon on the interannual time scale, but our results suggest a poor association between the ENSO (El Niño and La Niña) and the occurrence of dry and wet conditions in the MLSHD. Findings of García et al., (2005) reveal that ENSO influence is not significant on the P over Galicia. Though, according to Dai and Tan (2017), a warm (cold) ENSO enhances the negative (positive) AO phase, which is directly related to the MLSHD hydroclimate. Finally, the correlations between the SPEI1 to SPEI24 with WeMOi and EA are positive, but just statistically significant for the WeMOi with first two temporal scales of the SPEI.

Because the correlations in Figure 14a are greater with SPEI1 than with other temporal scales of this index, a second correlation analysis was conducted in order to determine the relationships between the SPEI1 and the teleconnections phenomena, but at monthly scale (Figure 14b). The correlations with the BEST index are mostly not statistically significant. Negative correlations only occur in spring (March, April, and May) (Figure 14b). Contrary, Muñoz-Díaz and Rodrigo (2004) found that the negative

phase of ENSO "La Niña" leads to a low probability of drought in spring, but for the whole north IP, while Lorenzo et al., (2010) also concluded that "La Niña" almost always announces dry springs in northwestern IP. Unlike these authors in this study we use an index that contemplates ocean and atmospheric conditions to identify the phases of the ENSO, and another index that contemplates both precipitation and evapotranspiration to identify drought conditions. In any case, this issue deserves further study.

The correlations obtained between the NAO and AO with SPEI1 are very similar (Figure 14b); however, as expected from the results already described for Figure 14a, it seems that the AO is best related with the SPEI1 variability, and consequently to monthly dry and wet conditions in the MLSHD throughout the hydrological year, especially in the winter and spring months (December to March). This in agreement with Mazano et al. (2019), who argued that the AO and NAO patterns have a significant impact on droughts in winter over large areas of the IP. However, at local and regional scale results may differ. In a previous study Rodriguez-Puebla and Nieto, (2010) revealed that positive (negative) NAO induce an east-west decreasing gradient of drier (wetter) conditions over the IP. Most recent findings of Sáez de Cámara et al., (2015) describe a complete lack of correlation between P anomalies and NAO for central and eastern north IP. These authors also shown that from the late 1980s to 2005 ocurred an increase in the frequency of extreme circulation modes within each NAO positive and negative phases, both inducing negative precipitation anomalies and long-lasting dry spell in north IP. That is, special care must be taken when associating a positive trend of the NAO with the increase of dry conditions in the entire IP. Positive correlations between the EA and SPEI1 are clearly observed from in the winter and spring months (November to May). Results of Casanueva et al. (2014) also revealed a positive correlation of EA with the P and the consecutive wet days over the northwest IP during the boreal winter. The SCAND pattern is also positively correlated during all months of the year, but no significant correlations were found in December, February, and March. This means that negative phase of the SCAND is related to dry conditions in the MLSHD. In the negative phase the European trough deepens, while weak pressure ridges are observed over the north eastern Atlantic Ocean. This make the Atlantic storm track extends north-eastwards affecting from a vast area from northern Europe to central Siberia (Bueh and Nakamura, 2007). Finally, the WeMOi shows positive significant correlations with SPEI1 from January to November, but specially in the boreal summer months. The WeMOi is particularly associated with the precipitation variability in the eastern part of the Iberian Peninsula and the south of France (Martín-Vide and Lopez-Bustins, 2006; Martin-Vide et al., 2008). However, these correlaions indicate that this index could be also useful to explain dry/wet conditions in the northwestern IP. The positive phase of the WeMO corresponds to the anticyclone over the Azores that may transport moisture entering the MSLHD from the west, and as previously explained the west circulation favours the occurrence of wet conditions in the MLSHD, in agreement with the positive correlations found. In its negative phase coincides the low-pressure often cut off from northern latitudes, in the framework of the Iberian south-west (Martín-Vide and Lopez-Bustins, 2006), possibly favouring the east circulation over the northwest IP, which also explain the positive correlation between WeMOi and SPEI1.

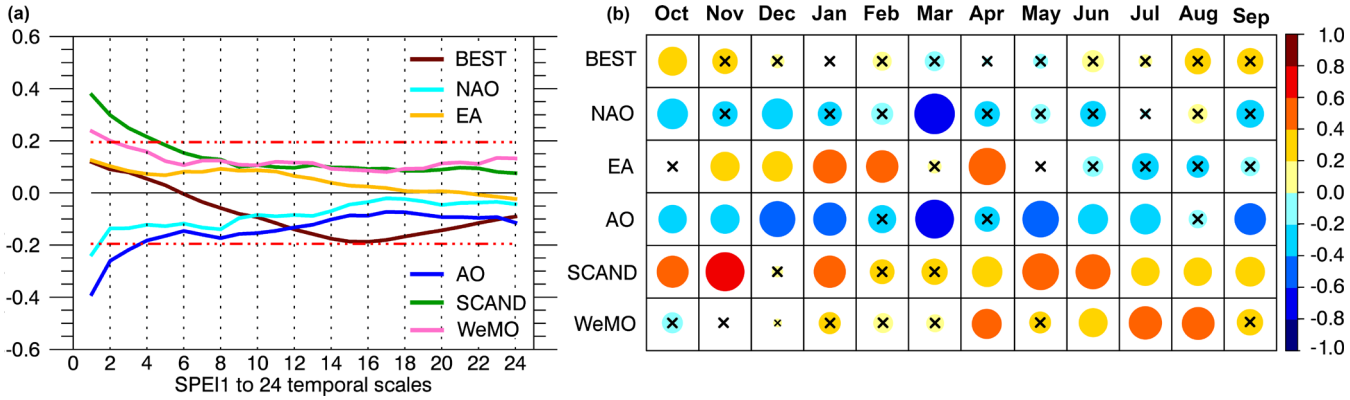

Figure 14. Correlation between the monthly series of the bivariate El Niño Southern Oscillation (BEST), North Atlantic Oscillation (NAO), East Atlantic (EA), Arctic Oscillation (AO) and Scandinavian Pattern (SCAND) and (WeMO) with monthly series of the SPEI1 to SPEI24 (a) and the monthly correlation between the same climatic indices and the SPEI1 (b) for the period 1980–2017. Not statistically significant correlations at 95% confidence level are those within discontinuous red lines in (a) and marked with an "x" in (b). The size of the circles is proportional to the correlation value.

The frequency bands and time intervals of the co-variations between SPEI1 and different modes of climate variability represented by climatic indices (i.e., BEST, EA, WeMOi, NAO, AO, and SCAND) is shown in Figure 15. The coloured shading displays the magnitude in the coherence as represented in the colour bar, which varies from 0 to 1 and indicates the timescale variability in the correlation between the two time series. Warmer colors (red) represent regions with significant interrelation, while colder colors (blue) signify lower dependence between the series. The results reveal that BEST shows strong but intermittently significant interannual coherence with SPEI1 in the period of the 1–7 months band. Besides a significant correlation is observed from 1980 to 1990 for the 40–60 months band, but it is outside the COI until the end of 1982. In this time scale the straight pointing down arrows indicates SPEI leads BEST by 90°. In the case of the EA there is a frequent, significant co-oscillation with the SPEI1 in the high-frequency 0–6 months band. However, from approximately the end of the 2000s to 2012, occurred a high coherence peak in the low-energy regions (for nearly 30–45 months). The coherence between SPEI1 and WeMOi expose frequent but not stationary interannual coherence regions at 1 – 8 months. At low frequencies (~ 64 months) is noticed strong positive coherence within the COI between 1992 – 2008.

Findings of Hurrell (1995) revealed that NAO has a rich combination of low frequencies from intraseasonal to interannual time scales, and low frequency from decadal to multidecadal time scales. In has significant coherence with the SPEI at high frequencies (6 to16 months) in the periods 1982–1984, 1986 and 2004–2012 (Figure 15), coinciding with dry periods in MLSHD. Strong coherence is also noticed at a longer temporal scale (30 months to 34 months) for the period 1986–1993. Results of Añel et al., (2005) also suggest that NAO and precipitation in Galicia could be also related at a time scale of 8 years. Compared with those in the NAO, oscillations in the AO are manifested in the SPEI1 over most of the period on intermittent

wavelengths from 2 months to 6 months, but most significantly and for longer periods in the range of 6 months to 36 months (3 years). In this frequency bands the left-pointing arrows show an anti-phase relationship (negative correlation), thereby indicating that the AO and SPEI1 moved in the opposite direction (when one is maximum, the other is minimum and vice versa). This is in accordance with previous correlations shown in Figure 14. Finally, the significant coherence between the SPEI1 and SCAND pattern reveals the influence of this teleconnections pattern between 1990 to 2005 along with the 0–8 months periodic bands and at low frequencies (from approximately 14 months to 40 months) during longer and continuous periods. Alternatively, arrows pointing to the right-down and right-up indicate but alternately the SPEI leads/lags the SCAND.

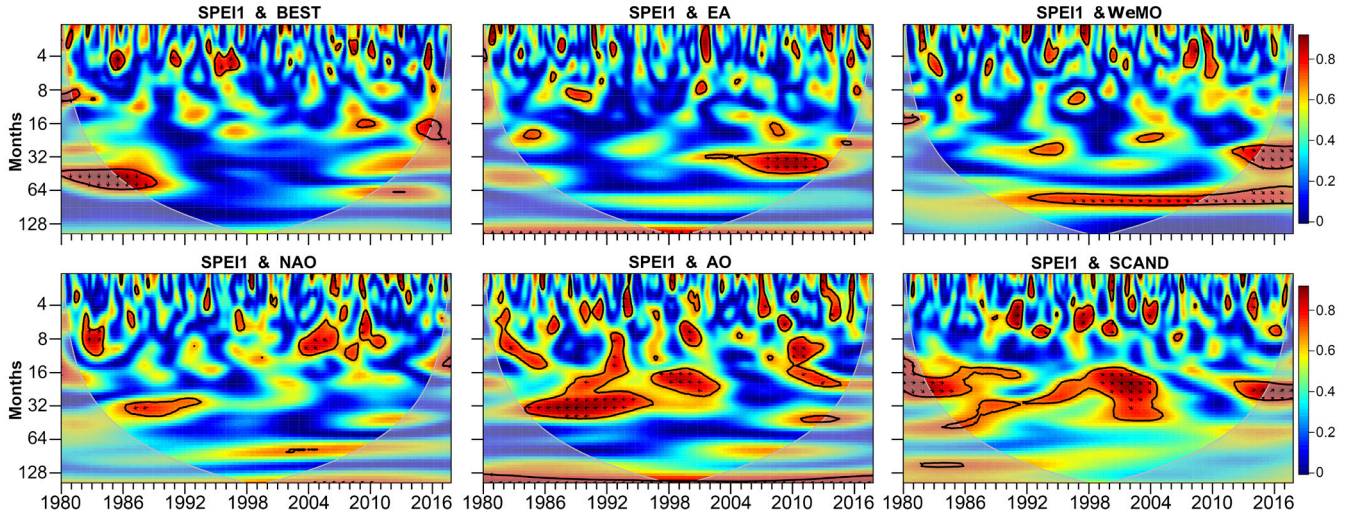

Figure 15. Wavelet coherence between the SPEI1 and the series of teleconnection patterns, namely the bivariate El Niño Southern Oscillation time series (BEST), East Atlantic (EA), North Atlantic Oscillation (NAO), Arctic Oscillation (AO), and Scandinavian Pattern (SCAND). The colours from blue to red indicate the increasing coherence. Areas enclosed by a black line correspond to statistically significant cross-wavelet powers at the 95% level. The grey line depicts the cone of influence (COI). The black arrows indicate the phase condition. The phase relationships between the climate indices and SPEI1 are denoted by arrows for in-phase pointing right, anti-phase pointing left, climate indices leading the SPEI1 by 90° pointing up, and SPEI1 leading the climate indices by 90° pointing down.

3.4 Hydrological drought

In figure 16 is observed the temporal evolution of the SRI for temporal scales of 1 (SRI1) and 6 (SRI6) months appears in figure 16. Negative values of the SRI indicate runoff droughts, normally recognised as hydrological drought. The high variability of SRI1 makes difficult to observe if occurred in continuous dry periods. The SRI6 depicts better the identification of continuous dry periods such as in 1991-1993; 2004-2005; 2011-2012 and the end of 2006 to 2007.

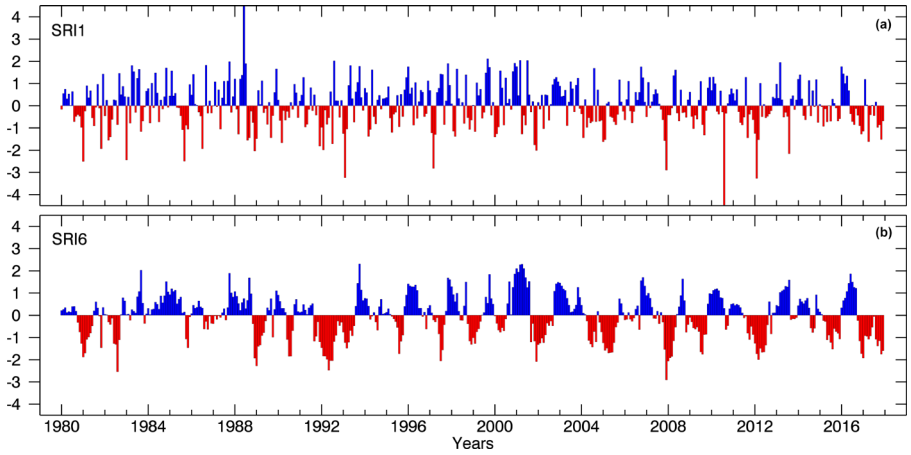

Figure 16. Temporal evolution of the Standardised Runoff Index computed for 1 (a) and 6 (b) months temporal scales in the MLSHD. Period 1980 – 2017.

A deficit in P coupled with higher evaporation rates leads to a meteorological drought that may propagate into the soil up to the crops, thereby leading to an agricultural drought and a hydrological drought when both the groundwater and streamflow are affected. However, drought propagation through every component of the hydrological cycle depends on the severity of drought as well as the characteristics of the catchments (Van Lanen, 2006; Wang et al., 2016). In this section we investigate the possible response of hydrological drought through the SRI computed at one month temporal scale, due to drought conditions considering the effect of current and previous drought conditions revealed by the SPEI1 to SPEI24 series. Correlations values in Figure 17a show that SRI1 variability is well associated with the first temporal scales (1 and 2 months) of the SPEI along all the hydrological year. However, hight correlations during all SPEI temporal scales highlight for December, January, and February, thereby suggesting that surface runoff during the rainiest months also depended on dry/wet conditions from previous months. From April to September the highest correlations are more restricted to the previous 2-4 months. According to a statistically significant correlation in July (the climatological driest month), the surface runoff variability is also affected by dry/wet conditions from the previous 4 – 21 months. Besides the SPEI is based in a water balance, the runoff seems that vary directly associated with the P annual cycle in the MLSHD. The maximum correlations in this figure indicate the best climatic time scale over which the runoff drought measured by the SRI, respond to dry/wet conditions according to the SPEI.

Figure 17b illustrates the monthly response rate (in percentage) of hydrological drought (SRI ≤ -0.84) to drought at different timescales according to SPEI1 to SPEI24 less or equal to -0.84. Dry conditions revealed at all temporal scales of the SPEI (1 – 2 months) have an outstanding different response rate of runoff drought across the hydrological year. The larger response (> 50%) occurs from October to April, and particularly in January, February and March (the rainiest months). In these months the rate of months under hydrological drought is also highly affected by drought conditions from several months ago. This is

in agreement with the correlation showed in Figure 17a. From May to Septemeber the P over the MLSHD decrease, and the rate response of runoff drought reach about 20%. This illustrates that runoff droughts are most linked to drought conditions in the same month during driest months of the year. A possible explanation to this is that evapotranspiration may be a determinant factor in the modulation of dry conditions during these months, and the runoff is more sensitive to rainfall.

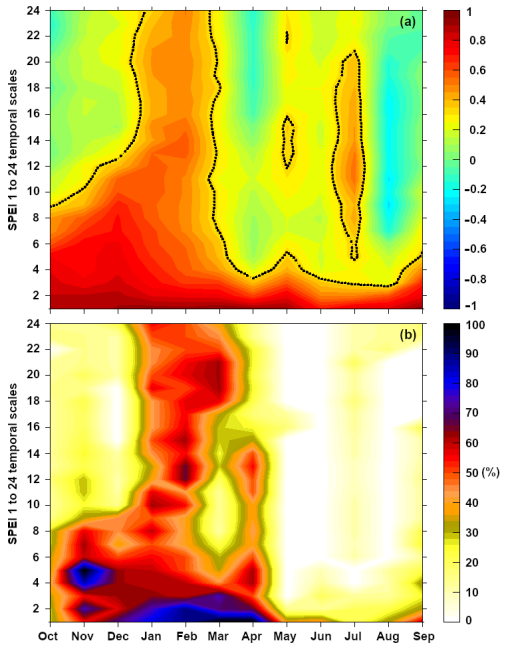

Figure 17. Monthly correlations among the Standardised Runoff Index (SRI) for the entire Miño-Limia-Sil Hydrographic Demarcation (MLSHD) with the Standardised Precipitation-Evapotranspiration Index (SPEI1 to SPEI24) in the MLSHD (a). Dotted lines represent significant correlations at $p < 0.05$. Rate (in percentage) of hydrological drought (SRI1 $\leq$ -0.84) during drought conditions according to monthly SPEI $\leq$ -0.84. Period 1980–2017.

4 Conclusions

In this study drought phenomenon in the MLSH has been investigated through the SPEI using high-resolution gridded datasets. An application of the Empirical Orthogonal Function method revealed highly homogeneous drought features despite the complex topography of the Demarcation. In the period of study frequent meteorological drought affected the MLSHD during 1989–1992, 2004–2007, and 2015–2017, while the most severe drought episodes during June/2016-January/2017, September/2011-March/2012, December/2014-August/2015, etc (Table 3). To investigate the atmospheric circulation associated with different drought categories in the MLSHD a WT classification for the entire IP was used. The results confirm previous findings for the northwest and the entire IP. The MLSHD is a hydroclimatic region where atmospheric circulation associated with weather types SW, W and NW (NE, E, SE) is related to wet (dry) conditions. A spatial correlation analysis

between ten pure WTs and the SPEI series computed on a one-month temporal scale revealed a highly uniform influence of every WT (and therefore the associated circulation) on the spatial variability of dry and wet conditions.

We found that dry/wet conditions in the MLSHD are susceptible to external forcings not only in short-term, but also for the mid-to-long-term changes. The most influential teleconnection patterns on dry/wet conditions variability in the MLSHD are the AO and SCAND, followed by the NAO, which is in agreement with previous results for the region. The signal of the AO and NAO are opposite to the SPEI1 in the MLSHD, while on the contrary, the SCAND is positively correlated with the SPEI1 series. Several studies have recognised the NAO as the dominant pattern for the Euro-Atlantic region. A deeper study on the short, medium and long term impact of NAO and AO on the atmospheric dynamics associated with hydrometeorological extremes in the northwest of the IP should be done. As well as the SCAND the WeMOi is positively correlated with the SPEI1 I the MLSHD. Intermitently significant coherence between the SPEI1 and other teleconnection patterns (BEST, EA) was also detected in the high-frequency region, but statistically significant correlations indicate there is not a great relationship of the ENSO event and the EA mode on the water balance at the MLSHD.

The SRI was used as a complement to the SPEI for representing hydrological drought in the MLSHD. We found that exists a fast propagation of meteorological drought to runoff drought across the year; normally at very short timescales (one, two months). However, this influence is higher in the climatological rainiest months of the year (winter months), when hydrological drought is affected even by previous 24 months of drought according to SPEI values less or equal to -0.84. This relationship is less observed in the dry season. In conclusion, this study provides some information that is fundamental to understand the climate forcing dry conditions in the MLSHD, which is an important hydrological and socioeconomic region of the north western IP. Furthermore, these results will support hydrometeorological forecasting and water management plans for the region.

Acknowledgments

R.S acknowledge the support from the European Union and FEDER thought the RISC-ML project under the INTERREG España-Portugal program. R.S and M.S acknowledge the grant received from the European Association for Territorial Cooperation, Galicia Northern Portugal (AECP, GNP) thought the IACOBUS program in 2019 and 2018 respectively. R.S and M.V are supported by the Xunta of Galicia under grants ED481B 2019/070 and ED481B 2018/062 respectively. M.L and M.S are supported by the project "Weather Extremes in the Euro Atlantic Region: Assessment and Impacts-WEx-Atlantic" (PTDC/CTA-MET/29233/2017). This work is part of the LAGRIMA project (RTI2018-095772-B-I00) funded by Ministerio de Ciencia, Innovación y Universidades, Spain. Partial support was also obtained from the Xunta de Galicia under the Project ED431C 2017/64-GRC "Programa de Consolidación e Estructuración de Unidades de Investigación Competitivas (Grupos de

Referencia Competitiva)". All the authors acknowledge the support of Dr. Alex Ramos from the Instituto Dom Luis for understanding the WTs computation.

References

1. Abatzoglou, J., Dobrowski, S., Parks, S.A., Hegewisch, K.C.: TerraClimate, a high-resolution global dataset of monthly climate and climatic water balance from 1958–2015. Sci. Data, 5, 170191. https://doi.org/10.1038/sdata.2017.191, 2018.
2. Abrantes, F., Rodrigues, T., Rufino, M., Salgueiro, E., Oliveira, D., Gomes, S., Oliveira, P., Costa, A., Mil-Homens, M., Drago, T., and Naughton, F.: The climate of the Common Era off the Iberian Peninsula, Clim. Past, 13, 1901–1918. https://doi.org/10.5194/cp-13-1901-2017, 2017.
3. Agnew, C.T.: Using the SPI to identify drought, Drought Netw. News 2000, 12, 6–12, http://digitalcommons.unl.edu/droughtnetnews/1, 2000.
4. Allen, R. G., Pereira, L. S., Raes, D., and Smith, M.: Crop evapotranspiration: Guidelines for computing crop water requirements. FAO Irrigation and Drainage Paper 56, 300 pp. www.fao.org/docrep/X0490E/X0490E00.htm, 1998.
5. Ambaum, M.H.P., Hoskins, B.J., and Stephenson, D.B: Arctic Oscillation or North Atlantic Oscillation?, J.Clim., 14, 3495-3507. https://doi.org/10.1175/1520-0442(2001)014<3495:AOONAO>2.0.CO;2, 2001.
6. Andrade, C., and Belo-Pereira, M.: Assessment of droughts in the Iberian Peninsula using the WASP Index. Atmos. Sci. Lett., 16, 208-218. https://doi.org/10.1002/asl2.542, 2015.
7. Añel, J.A., Blanco-Durán, M., Gimeno, L., de la Torre, L.: Recovery of Meteorological Data for the Observatory of A Guarda, Spain. PLOS ONE 7(6), e39281. https://doi.org/10.1371/journal.pone.0039281, 2012.
8. Awan, J.A., Bae, D-H. and Kim, K-J. : Identification and trend analysis of homogeneous rainfall zones over the East Asia monsoon region. Int. J. Climatol., 35, 1422-1433. https://doi.org/10.1002/joc.4066, 2015.
9. Barbeta, A., and Peñuelas, J.: Sequence of plant responses to droughts of different timescales: lessons from holm oak (Quercus ilex) forests, Plant. Ecol. Divers., 1-18, https://doi.org/10.1080/17550874.2016.1212288, 2016.
10. Barnston, A.G., and Livezey, R.E.: Classification, Seasonality and Persistence of Low-Frequency Atmospheric Circulation Patterns, Mon. Weather Rev., 115, 1083-1126. https://doi.org/10.1175/1520-0493(1987)115<1083:CSAPOL>2.0.CO;2, 1987.
11. Bharath, R., Srinivas, V.V.: Delineation of homogeneous hydrometeorological regions using wavelet based global fuzzy cluster analysis. Int. J. Climatol., 35, 4707-4727. https://doi.org/10.1002/joc.4318, 2015.
12. Bittelli, M., Ventura, F., Campbell, G.S., Snyder, R.L., Gallegati, F., Pisa, P.R.: Coupling of heat, water vapor, and liquid water fluxes to compute evaporation in bare soils. J. Hydrol. 362(3–4), 191–205. https://doi.org/10.1016/j.jhydrol.2008.08.014, 2008.

13. Bueh, C., and Nakamura, H.: Scandinavian pattern and its climatic impact, Q. J. R. Meteorol. Soc., 133, 2117-2131, https://doi.org/10.1002/qj.173, 2017.
14. Casanueva, A., Rodríguez-Puebla, C., Frías, M.D., and González-Reviriego, N.: Variability of extreme precipitation over Europe and its relationships with teleconnection patterns. Hydrol. Earth Syst. Sci., 18, 709–725, https://doi.org/10.5194/hess-18-709-2014, 2014.
15. CA (Convenção Albufeira). http://www.cadc-albufeira.eu/pt/cuencas-hidrograficas/cuenca-limia/, acceced on February 22, 2020.
16. Cornes, R., van der Schrier, G. van den Besselaar, E.J.M., and Jones. P.D.: An Ensemble Version of the E-OBS Temperature and Precipitation Datasets, J. Geophys. Res. Atmos., 123, 1-52, https://doi.org/10.1029/2017JD028200, 2018.
17. Cortesi, N., Gonzalez-Hidalgo, J.C., Trigo, R.M., and Ramos, A.M.: Weather Types and spatial variability of precipitation in the Iberian Peninsula, Int. J. Climatol., 34, 2661-2677, https://doi.org/10.1002/joc.3866, 2014.
18. Dai, A.: Characteristics and trends in various forms of the Palmer Drought Severity Index during 1900–2008. J. Geophys. Res., 116, D12115, https://doi.org/10.1029/2010JD015541, 2011
19. Dai, P., Tan, B.: The Nature of the Arctic Oscillation and Diversity of the Extreme Surface Weather Anomalies It Generates. J. Climate, 30, 5563–5584, https://doi.org/10.1175/JCLI-D-16-0467.1, 2017.
20. Davarzani, H., Smits, K., Tolene, R. M., Illangasekare, T.: Study of the effect of wind speed on evaporation from soil through integrated modeling of the atmospheric boundary layer and shallow subsurface. Water resources research, 50(1), 661–680, https://doi.org/10.1002/2013WR013952, 2014.
21. deCastro, M., Lorenzo, N.G., Taboada, J.J., Sarmiento, M.E., Alvarez, I., and Gómez-Gesteira, M.: Influence of teleconnection patterns on precipitation variability and on river flow regimes in the Miño River basin (NW Iberian Peninsula), Clim. Res., 32, 63-73, https://doi.org/doi:10.3354/cr032063 , 2006.
22. Dee, D.P., Uppala, S.M., Simmons, A.J., Berrisford, P., Poli, P., Kobayashi, S., Andrae, U., Balmaseda, M.A., Balsamo, G., Bauer, P., et al.: The ERA-Interim reanalysis: Configuration and performance of the data assimilation system. Q. J. R. Meteorol. Soc. 137, 553–597, https://doi.org/10.1002/qj.828, 2001.
23. Drumond, A., Nieto, R., Gimeno, L., Vicente-Serrano, S.M., and Lopez-Moreno, J.I.: Characterization of the atmospheric component of the winter hydrological cycle in the Galicia/North Portugal Euro-region: a Lagrangian approach, Clim. Res., 48, 193-201, https://doi.org/10.3354/cr00987, 2011.
24. Enfield, D.B., Mestas-Nunez, A.M., and Trimble, P.J.: The Atlantic Multidecadal Oscillation and its relationship to rainfall and river flows in the continental U.S., Geophys. Res. Lett., 28, 2077-2080, http://dx.doi.org/10.1029/2000GL012745, 2001.
25. García, N.O., Gimeno, L., de la Torre, L., Nieto, R., Añel, J.A.: North Atlantic Oscillation (NAO) and precipitation in Galicia (Spain). Atmósfera, 18(1), 25-32, 2005.

26. García-Herrera, R., Hernández, E. Barriopedro, D. Paredes, D. Trigo, R.M., Trigo, I.F.,and Mendes, M.A.: The Outstanding 2004/05 Drought in the Iberian Peninsula: Associated Atmospheric Circulation, J. Hydrometeor., 8, 483–498, https://doi.org/10.1175/JHM578.1, 2007.
27. Gerber, N., and Mirzabaev, A.: Benefits of Action and Costs of Inaction: Drought Mitigation and Preparedness-A Literature Review, Technical report, World Meteorological Organization (WMO) and Global Water Partnership (GWP), https://doi.org/10.1201/9781315265551-8,2017.
28. Grinsted, A., Moore, J.C., and Jevrejeva, S.: Application of the cross wavelet transform and wavelet coherence to geophysical time series, Nonlin. Processes Geophys., 11, 561-566, https://doi.org/10.5194/npg-11-561-2004, 2004.
29. Gómez-Gesteira, M., Gimeno, L., deCastro M., Lorenzo, M.N., Alverez, I., Nieto, R., Taboada, J.J., Crespo, A.J.C., Ramos, A.M., Iglesias, I., Gómez-Gesteira, J.L., Sanro, F.E., Barriopedro, D., and Trigo, I.F.: The state of climate in NW Iberia. Clim. Res., 48, 109-144, https://doi.org/10.3354/cr00967, 2011.
30. González-Hidalgo, J.C., Vicente-Serrano, S.M., Peña-Angulo, D., Salinas, M., Tomas-Burguera, S., and Begueria, S.: High-resolution spatio-temporal analyses of drought episodes in the western Mediterranean basin (Spanish mainland, Iberian Peninsula). Acta Geophys., 66: 381-392, https://doi.org/10.1007/s11600-018-0138-x, 2018.
31. Gouveia, C., Trigo, R. M., and DaCamara, C. C.: Drought and vegetation stress monitoring in Portugal using satellite data, Nat. Hazards Earth Syst. Sci., 9, 185-195, https://doi.org/10.5194/nhess-9-185-2009, 2009.
32. Guerreiro, S.B., Dawson, R.J., Kilsby, C., Lewis, E., and Ford, A.: Future heat-waves,droughts and floods in 571 European cities, Environ. Res. Lett., 13, 1-11, https://doi.org/10.1088/1748-9326/aaaad3, 2018.
33. Hargreaves, G. H., and Samani, Z.: Reference crop evapotranspiration from temperature, Appl. Eng. Agric., 1, 96–99, https://doi.org/10.13031/2013.26773, 1985.
34. Hénin, R., Ramos, A.M., Schemm, S., Gouveia., C.M., Liberato, M.L.R.: Assigning precipitation to mid-latitudes fronts on sub-daily scales in the North Atlantic and European sector: Climatology and trends. Int. J. Climatol. 39, 317–330. https://doi.org/10.1002/joc.5808, 2019.
35. Hurrell, J.W.: Decadal trends in the North Atlantic Oscillation and relationships to regional temperature and precipitation, Science, 269, 676-679 , https://doi.org/10.1126/science.269.5224.676, 1995.
36. IPCC, 2018: Summary for Policymakers. In: Global Warming of 1.5°C. An IPCC Special Report on the impacts of global warming of 1.5°C above pre-industrial levels and related global greenhouse gas emission pathways, in the context of strengthening the global response to the threat of climate change, sustainable development, and efforts to eradicate poverty [Masson-Delmotte, V., P. Zhai, H.-O. Pörtner, D. Roberts, J. Skea, P.R. Shukla, A. Pirani, W. Moufouma-Okia, C. Péan, R. Pidcock, S. Connors, J.B.R. Matthews, Y. Chen, X. Zhou, M.I. Gomis, E. Lonnoy, T. Maycock, M. Tignor, and T. Waterfield (eds.)]. World Meteorological Organization, Geneva, Switzerland, 32 pp.
37. Knapp, A.K., Carroll, C.J.W., Denton, E.M., La Pierre, K.J., Collins, S.L., and Smith, M.D.: Differential sensitivity to regional-scale drought in six central US grasslands, Oecologia, 177, 949-957, https://doi.org/10.1007/s00442-015-3233-6, 2015.

38. Knudsen, M. F., Seidenkrantz, M.S., Jacobsen, B. H., and Kuijpers, A.: Tracking the Atlantic Multidecadal Oscillation through the last 8000 years, Nat. Commun., 2, 1-8, https://doi.org/10.1038/ncomms1186, 2011.
39. Patakamuri, S.K., and O'Brien, N.: Modified Versions of Mann Kendall and Spearman's Rho Trend Tests version 1.4.0, https://cran.r-project.org/web/packages/modifiedmk/modifiedmk.pdf, 2019.
40. Lana, X., Martínez, M. D., Burgueño, A., Serra, C., Martín-Vide, J., and Gómez, L.: Distributions of long dry spells in the iberian peninsula, years 1951–1990, Int. J. Climatol., 26, 1999-2021, https://doi.org/10.1002/joc.1354, 2006.
41. Lehner, B., Verdin, K., and Jarvis, A.: New global hydrography de-rived from spaceborne elevation data, Eos, Transactions,89, 93–94, https://doi.org/10.1029/2008EO100001,2011.
42. Liberato, M.L.R., Ramos, A.M., Gouveia, C.M., Sousa, P., Russo, A., Trigo, R.M., Santo, F.E.: Exceptionally extreme drought in Madeira Archipelago in 2012: Vegetation impacts and driving conditions.Agricultural and Forest Meteorology, 232, 195-209. https://doi.org/10.1016/j.agrformet.2016.08.010, 2017.
43. Lorenzo-Lacruz, J., Morán-Tejeda, E., Vicente-Serrano, S. M., and López-Moreno, J. I.: Streamflow droughts in the Iberian Peninsula between 1945 and 2005: spatial and temporal patterns, Hydrol. Earth Syst. Sci., 17, 119-134, https://doi.org/10.5194/hess-17-119-2013, 2013.
44. López-Moreno, J. I., Vicente-Serrano, S.M., Zabalza, J., Begueria, S., Lorenzo-Lacruz, J., Azorin-Molina, C., and Morán-Tejeda, E.: Hydrological response to climate variability at different time scales: a study in the Ebro basin, J. Hydrol., 477, 175–188, https://doi.org/10.1016/j.jhydrol.2012.11.028, 2013.
45. Mallants, D., Feyen, J.: Defining Homogeneous Precipitation Regions by Means of Principal Components Analysis. J. Appl. Meteor., 29, 892–901, https://doi.org/10.1175/1520-0450(1990)029<0892:DHPRBM>2.0.CO;2,1990.
46. Martens, B., Miralles, D.G., Lievens, H., van der Schalie, R., de Jeu, R.A.M., Fernández-Prieto, D., Beck, H.E., Dorigo, W.A., and Verhoest, N.E.C.: GLEAM v3: satellite-based land evaporation and root-zone soil moisture, Geosci. Model Dev., 10, 1903–1925, https://doi.org/10.5194/gmd-10-1903-2017, 2017.
47. Martín-Vide, J., Lopez-Bustins, J.A.: The Western Mediterranean Oscillation and rainfall in the Iberian Peninsula. Int. J. Climatol., 26 (11), 1455-1475. https://doi.org/10.1002/joc.1388, 2006.
48. McKee, T. B. N., Doesken, J., and Kleist, J.: The relationship of drought frequency and duration to time scales, Eight Conf. On Applied Climatology, Anaheim, California, United States, 179-184, 1993.
49. McMichael, A.J, and Lindgren, E.: Climate change: present and future risks to health, and necessary responses, J. Intern. Med., 270, 401-413, https://doi.org/10.1111/j.1365-2796.2011.02415.x, 2011.
50. Miralles, D.G., Holmes, T.R.H., de Jeu, R.A.M., Gash, J.H., Meesters, A.G.C.A., Dolman, A.J.: Global land-surface evaporation estimated from satellite-based observations, Hydrol. Earth Syst. Sci., 15, 453–469, doi: 10.5194/hess-15-453-2011, 2011.
51. Mora Aliseda, J., Garrido Velarde, J., Díaz González, M.: Dinámicas socio-espaciales y previsiones demográficas en la cuenca internacional del Miño-Sil. Anales De Geografía De La Universidad Complutense, 35(1), 95-117, https://doi.org/10.5209/rev_AGUC.2015.v35.n1.48965, 2015.

52. Muñoz-Díaz, D., and Rodrigo, F. S.: Influence of the El Niño-Southern Oscillation on the probability of dry and wet seasons in Spain, Clim. Res., 30, 1–12, https://doi.org/10.3354/cr030001, 2004.
53. Ojeda, M. G-V., Jiménez,E.R., Gámiz-Fortis, S.R., Castro-Díez, Y., and Esteban Parra, M.J.: Understanding the Drought Phenomenon in the Iberian Peninsula, In book: Drought (Aridity) , https://doi.org/10.5772/intechopen.85472, 2019.
54. Paredes, D., Trigo, R.M., Garcia-Herrera, R., Trigo, I.F.: Understanding Precipitation Changes in Iberia in Early Spring: Weather Typing and Storm-Tracking Approaches. J. Hydrometeor., 7, 101–113, https://doi.org/10.1175/JHM472.1, 2006.
55. Parracho, A.C., Gonçalves, P.M., and Rocha, A.: Regionalisation of precipitation for the Iberian Peninsula and climate change, Phys. Chem. Earth, 54, 146-154, https://doi.org/10.1016/j.pce.2015.07.004, 2016.
56. Páscoa, P., Gouveia, C. M., Russo, A., and Trigo, R. M.: Drought Trends in the Iberian Peninsula over the Last 112 Years, Adv. Meteorol., 1-13, https://doi.org/10.1155/2017/4653126, 2017.
57. Peña-Gallardo, M., Vicente-Serrano, S.M., Camarero, J.J., Gazol, A., Sánchez-Salguero, R., Domínguez-Castro, F., El Kenawy, A., Beguería-Portugés, S., Gutiérrez, E., De Luis, M., Sangüesa-Barreda, G., Novak, K., Rozas, V., Tíscar, P.A., Linares, J.C., Martínez del Castillo, E., Ribas Matamoros, M., García-González, I., Silla, F., Camisón, Á., Génova, M., Olano, J.M., Longares, L.A., Hevia, A., and Galván, J.D.: Drought Sensitiveness on Forest Growth in Peninsular Spain and the Balearic Islands, Forests, 9, 1-20, https://doi.org/10.3390/f9090524, 2018.
58. Peña-Gallardo, M., Vicente-Serrano, S. M., Domínguez-Castro, F., and Beguería, S.: The impact of drought on the productivity of two rainfed crops in Spain, Nat. Hazards Earth Syst. Sci., 19, 1215-1234, https://doi.org/10.5194/nhess-19-1215-2019, 2019.
59. PES. Plan especial de actuación en situaciones de alerta y eventual sequía, 2017. Documento Ambiental Estratégico, Confederación Hidrográfica del Miño-Sil, https://www.chminosil.es.
60. Preisendorfer, R.W., Mobley, C.D.: Principal component analysis in meteorology and oceanography. Elsevier, Amsterdam, pp. 425. 1988.
61. Ramos, A.M., Cortesi, N., and Trigo, R.M.: Circulation weather types and spatial variability of daily precipitation in the Iberian Peninsula. Front. Earth Sci., 2, 1-17, https://doi.org/10.3389/feart.2014.00025, 2014.
62. Rivière, G., and Drouard, M.: Dynamics of the Northern Annular Mode at Weekly Time Scales, J. Atmos. Sci., 72, 4569–4590, https://doi.org/10.1175/JAS-D-15-0069.1, 2015.
63. Rodriguez-Puebla, C., Encinas, A.H., Nieto, S., and Garmendia, J.: Spatial and temporal patterns of annual precipitation variability over the Iberian Peninsula. Int. J. Climatol., 18, 299-316, https://doi.org/10.1002/(SICI)1097-0088(19980315)18:3<299::AID-JOC247>3.0.CO;2-L, 1998.
64. Russo, C., Gouveia, M., Trigo, R. M., Liberato, M. L., and DaCamara, C. C.: The influence of circulation weather patterns at different spatial scales on drought variability in the Iberian Peninsula, Front. Environ. Sci., 3, 1-15, https://doi.org/10.3389/fenvs.2015.00001, 2015 .

65. Salvador, C., Nieto, R., Linares, C., Díaz, J., and Gimeno, L.: Effects on daily mortality of droughts in Galicia (NW Spain) from 1983 to 2013, Sci. Total Environ., 662, 121-133, https://doi.org/10.1016/j.scitotenv.2019.01.217, 2019.
66. Schulte, E.M.m Grilo, C.M., and Gearhardt, A.N.: Shared and unique mechanisms underlying binge eating disorder and addictive disorders, Clin. Psychol. Rev., 44, 125-139, https://doi.org/10.1016/j.cpr.2016.02.001, 2016.
67. Seneviratne, S.: Historical drought trends revisited. Nature, 491, 338–339, https://doi.org/10.1038/491338a, 2012.
68. Serrano, A., García, J.A., Mateus, V.L., Cancillo, M.L., and Garrido, J.: Monthly modes of variation of precipitation over the Iberian Peninsula, J. Clim., 12, 2894-2919, https://doi.org/10.1175/1520-0442(1999)012<2894:MMOVOP>2.0.CO;2, 1999.
69. Smith, C.A., and Sardeshmukh, P.: The Effect of ENSO on the Intraseasonal Variance of Surface Temperature in Winter, Int. J. Climatol., 20, 1543 1557, https://doi.org/10.1002/1097-0088(20001115)20:13<1543::AID-JOC579>3.0.CO;2-A, 2000.
70. Sousa, P. M., Barriopedro, D., Trigo, R.M., Ramos, A.M., Nieto, R., Gimeno, L., Turkman, K. F., and Liberato, M.L.R.: Impact of Euro-Atlantic blocking patterns in Iberia precipitation using a novel high resolution dataset, Clim. Dyn., 46, 2573–2591, https://doi.org/10.1007/s00382-015-2718-7, 2016.
71. Spinoni, J., Naumann, G., Vogt, J., and Barbosa, P.: Meteorological droughts in Europe, Events and impacts, past trends and future projections, Publications Office of the European Union, Luxembourg, EUR 27748 EN, 129 pp., https://doi.org/10.2788/450449, 2016.
72. Spinoni, J., Vogt, J.V., Naumann, G., Barbosa, P., Dosio, A.: Will drought events become more frequent and severe in Europe?. Int. J. Climatol, 38, 1718-1736, https://doi.org/10.1002/joc.5291, 2018.
73. Stanke, C., Kerac, M., Prudhomme, C., Medlock, J., and Murray, V.: Health effects of drought: a systematic review of the evidence. PLoS Curr., 5, 1-22, https://doi.org/10.1371/currents.dis.7a2cee9e980f91ad7697b570bcc4b004, 2013.
74. Svoboda, M., Fuchs, B.: Handbook of Drought Indicators and Indices; World Meteorological Organization (WMO): Geneva, Switzerland; Global Water Partnership (GWP): Geneva, Switzerland, pp. 1–45 2016.
75. Thompson, D. W. J., and Wallace, J. M.: The Arctic Oscillation signature in the wintertime geopotential height and temperature fields, Geophys. Res. Lett., 25, 1297-1300, https://doi.org/10.1029/98GL00950, 1998.
76. Tomas-Burguera, M., Vicente-Serrano, S.M., Grimalt, M., Begueria, S.: Accuracy of reference evapotranspiration (ET0) estimates under data scarcity scenarios in the Iberian peninsula. Agric. Water Manage., 182, 103-116, https://doi.org/10.1016/j.agwat.2016.12.013, 2017.
77. Torrence, C. G., and Compo, P.: A practical guide to wavelet analysis. Bulletin of the American Meteorological Society, 79, 1, pp. 61–78, 1998.
78. Torrence, C. and Webster, P.J.: Interdecadal Changes in the ENSO–Monsoon System, J. Clim., 12, 2679–2690, https://doi.org/10.1175/1520-0442(1999)012<2679:ICITEM>2.0.CO;2, 1999.

79. Trenberth, K.E., Dai, A., Schrier, G., Jones, P.D., Barichivich, J., Briffa, K.R. and Sheffield, J. Global warming and changes in drought, Nat. Clim. Change, 4, 17– 22, https://doi.org/10.1038/nclimate2067, 2014.
80. Trigo, R.M., and DaCamara, CC.: Circulation weather types and their influence on the precipitation regime in Portugal, Int. J. Climatol., 20, 1559–1581, https://doi.org/10.1002/1097-0088(20001115)20:13<1559::AID-JOC555>3.0.CO;2-5, 2000.
81. Trigo, R.M., Osborn, T.J., and Corte-Real, J.: The North Atlantic Oscillation influence on Europe: Climate impacts and associated physical mechanisms, Clim., Res., 20, 9-17, https://doi.org/10.3354/cr020009, 2002.
82. Trigo, R. M., Pozo-Vázquez, D., Osborn, T. J., Castro-Díez, Y., Gámiz-Fortis, S., and Esteban-Parra, M. J.: North Atlantic oscillation influence on precipitation, river flow and water resources in the Iberian Peninsula. Int. J. Climatol., 24, 925-944, https://doi.org/doi:10.1002/joc.1048, 2004.
83. UN.: Drainage basins of the North Sea and Eastern Atlantic, Chapter 7, in: Second Assessment of Transboundary Rivers, Lakes and Groundwaters, UN, New York, https://doi.org/10.18356/57863ad2-en, 182-215, 2011.
84. Van Lanen, H.A.J.: Drought propagation through the hydrological cycle. Climate Variability and Change—Hydrological Impacts, in: Proceedings of the Fifth FRIEND World Conference , Havana, Cuba, November, 2006, 308, 2006.
85. Van Loon, A.F., Stahl, K., Di Baldassarre, G., Clark, J., Rangecroft, S., Wanders, N., Gleeson, T., Van Dijk, A. I. J.M., Tallaksen, L.M., Hannaford, J., Uijlenhoet, R., Teuling, A.J., Hannah, D.M., Sheffield, J., Svoboda, M., Verbeiren, B., Wagener, T., Van Lanen, H.A.J.: Drought in a human-modified world: reframing drought definitions, understanding, and analysis approaches. Hydrol. Earth Syst. Sci., 20, 3631–3650, https://doi.org/10.5194/hess-20-3631-2016, 2016.
86. Vargas, J., and Paneque, P.: Challenges for the Integration of Water Resource and Drought-Risk Management in Spain, Sustainability, 11, 1-16, https://doi.org/10.3390/su11020308, 2019.
87. Martin-Vide, J., and Lopez-Bustins, J.-A.: The Western Mediterranean Oscillation and rainfall in the Iberian Peninsula. Int. J. Climatol., 26, 1455-1475, doi:10.1002/joc.1388, 2006.
88. Martin-Vide, J., Sanchez-Lorenzo, A., Lopez-Bustins, J.A., Cordobilla, M.J., Garcia-Manuel, A., and Raso, J.M.: Torrential rainfall in northeast of the Iberian Peninsula: synoptic patterns and WeMO influence.Advances in Science and Research, Copernicus Publications, 2008, 2, pp.99-105. hal-00297465.
89. Vicente-Serrano, S.M., Beguería, S., and López-Moreno, J.I.: A Multiscalar Drought Index Sensitive to Global Warming: The Standardized Precipitation Evapotranspiration Index, J. Clim., 23, 1696–1718, https://doi.org/10.1175/2009JCLI2909.1, 2010.
90. Vicente-Serrano, S. M.: El Niño and La Niña influence on droughts at different timescales in the Iberian Peninsula, Water Resour. Res., 41, 1-18, https://doi.org/10.1029/2004WR003908, 2005.
91. Vicente-Serrano, S. M., López-Moreno, J. I., Bergueria, S., Lorenzo-Lacruz, J., Sanchez-Lorenzo, A., García-Ruiz, J.M., Azorin-Molina, Morán-Tejeda, E., Revuelto, J., and Trigo, R.: Evidence of increasing drought severity caused

by temperature rise in southern Europe, Environ. Res. Lett., 9, 1-14, https://doi.org/10.1088/1748-9326/9/4/044001, 2014.

92. Vicente-Serrano, S.M., López-Moreno, J.I., Drumond, A., and Gimeno, L., Nieto, R., Morán-Tejeda, E., Lorenzo-Lacruz, J., Begueria, S., and Zabalza, J.: Effects of warming processes on droughts and water resources in the NW Iberian -Peninsula (1930−2006). Clim. Res., 48, 203-212, https://doi.org/10.3354/cr01002, 2011.
93. Vicente-Serrano, S.M., López-Moreno, J.I., Santiago, B., Lorenzo-Lacruz, J., Azorin-Molina, C., and Morán-Tejeda, E.: Accurate computation of a streamflow drought index, J. Hydrol. Eng., 17, 318–332, https://doi.org/10.1061/%28ASCE%29HE.1943-5584.0000433, 2012.
94. Vidal-Macua J.J., Ninyerola M., Zabala A., Domingo-Mari-mon C., and Pons, X.: Factors affecting forest dynamics in the Iberian Peninsula from 1987 to 2012. The role of topography and drought, For. Ecol. Manag., 406, 290–306, https://doi.org/10.1016/j.foreco.2017.10.011, 2017.
95. Visbeck, M.H., Hurrell, J.W., Polvani, L., Cullen, H.M.: The North Atlantic Oscillation: Past, present, and future, Proc. Natl. Acad. Sci. U.S.A., 98, 12876-2877, https://doi.org/10.1073/pnas.231391598, 2001.
96. Von Storch, H., Navarra, A.: Spatial patterns: EOFs and CCA. In: Von Storch H, Navarra A (eds) Analysis of climate variability: application of statistical techniques Springer, New York, 227–258, https://doi.org/10.1007/978-3-662-03167-4, 1995.
97. Wang, W., Ertsen, M.W., Svoboda, M.D., Hafeez, M.: Propagation of Drought: From Meteorological Drought to Agricultural and Hydrological Drought, Adv. Meteorol., 2016, 1-5, http://dx.doi.org/10.1155/2016/6547209, 2016.
98. Wang, H., Pan, Y., Chen, Y.: Comparison of three drought indices and their evolutionary characteristics in the arid region of northwestern China. Atmos. Sci. Lett, 18, 132-139, http://dx.doi.org/10.1002/asl.735, 2017.
99. Wang, Y., Quan, Q., Shen B.: Spatio-temporal variability of drought and effect of large scale climate in the source region of Yellow River, Geomatics, Natural Hazards and Risk, 10(1), 678-698, http://dx.doi.org/10.1080/19475705.2018.1541827, 2019.
100. Wanner, H., Brönnimann, S., Casty, C., Gyalistras, D., Luterbacher, J., Schmutz, C., Stephenson, D.B., and Xoplaki, E.: North Atlantic Oscillation – Concepts and Studies, Surv. Geophys., 22, 321–381, https://doi.org/10.1023/A:1014217317898, 2001.
101. Wehrli, K., Guillod, B.P., Hauser, M., Leclair, M., Seneviratne, S.I.: Assessing the dynamic versus thermodynamic origin of climate model biases. Geophysical Research Letters, 45, 8471-8479, https://doi.org/10.1029/2018GL079220, 2018.
102. Wilhite, D. A.: Drought as a Natural Hazard: Concepts and Definitions. Drought: A Global Assessment, edited by Wilhite, D.A., Natural Hazards and Disasters Series, Routledge, London, U.K., 3-18, 2000.
103. World Meteorological Organization. Standardized Precipitation Index User Guide. 2012. Available online: http://www.wamis.org/agm/pubs/SPI/WMO_1090_EN.pdf (accessed on 08 September 2019).

104. World Meteorological Organization (WMO) and Global Water Partnership (GWP), 2016: Handbook of Drought Indicators and Indices (M. Svoboda and B.A. Fuchs). Integrated Drought Management Programme (IDMP), Integrated Drought Management Tools and Guidelines Series 2. Geneva.